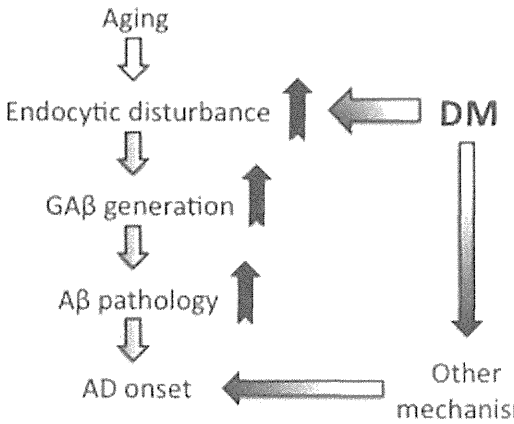

Fig 7. Hypothetical schema of DM-induced Aβ pathology leading to AD onset. From the results of this study, we propose that DM induces GAβ generation by exacerbating age-dependent endocytic disturbance, resulting in enhanced Aβ pathology in the brain. Although additional studies are needed to clarify the whole mechanisms underlying DM-associated pathology, we hypothesize that, at the very least, enhanced Aβ pathology accompanied by endocytic disturbance might be involved in the development of AD.

doi:10.1371/journal.pone.0117362.g007

monkeys. Moreover, the result of this study also suggests that enhanced Aβ aggregation could induce SP deposition without significant changes in total Aβ level. Relevant to proposed AD pathophysiogical mechanisms, we also observed apparent endocytic pathology, including enlarged early endosomes and APP accumulation in neurons of DM-affected adult monkeys (Fig. 5A-E). Western blot analyses confirmed a significant increase of Rab GTPases in these brains at nearly the same level as in aged monkey brains (Fig. 5F, G). Our previous studies showed that an increase in Rab GTPases is a good indicator for alterations in intracellular endosome trafficking associated with a particular Rab GTPase [45, 46]. Indeed, increased Rab GTPase levels are strongly associated with endocytic disturbance [45, 46]. The observation that experimentally induced disorders of the endocytic pathway cause GAβ-dependent Aβ pathology [34, 52] supports the premise that endocytic disturbance is likely responsible for enhanced GAβ generation. Along these lines, we surmise that intracellular endosome trafficking would be altered in the brains of DM-affected adult monkeys, resulting in severe endocytic disturbance, as observed in aged monkey brains. This might be why GAβ generation was enhanced, thereby inducing SP deposition (Fig. 2). Moreover, the results of this study strongly support the idea that endocytic disturbance is essentially involved in the development of AD pathology [33, 34, 42–45].

A recent study showed that the expression of axonal transport motor proteins was altered in experimentally DM-induced rodent model, and axonal transport motor proteins are indeed required for endosome trafficking [48, 49]. However, in the present study, we did not find any changes in axonal motor protein levels, suggesting that the mechanism underlying endocytic disturbance in the brains of DM-affected adult monkeys would be independent of axonal motor protein levels. Previous finding showed that the breakdown in lysosomal degradation also induces endocytic disturbance [50]. In DM-affected adult monkey brains, the level of CatD heavy chain increased in DM-affected adult monkey brains, indicating that the endosomal-lysosomal system is activated as such in AD patient brains (Fig. 6) [53]. This finding suggests that DM really enhances AD pathology. On the other hand, we observed the significant increase in autophagosome marker LC3-II level in DM-affected adult monkey brains (Fig. 6). Since LC3-I level was unchanged, the induction of autophagy was not altered, but lysosomal-

autophagosome clearance was likely disturbed in DM-affected adult monkey brains (Fig. 6). The defective lysosomal-autophagosome clearance is associated with AD pathology [50, 54–56], and the result of this study is also consistent with a previous finding that the aberrant lysosomal-autophagic turnover is associated with the accumulation of GAβ in rodent brain [57].

Given that CatD heavy chain level was increased, i.e. lysosomal degradation was induced (Fig. 6), the disturbance in the fusion of autophagosome and lysosome might be responsible for impaired lysosomal-autophagosome clearance in DM-affected adult monkey brains. The fusion step is indispensable for lysosomal-autophagosome clearance [58, 59] and mediated by Rab7 [60]. In DM-affected adult monkey brains, Rab7 level was obviously increased as compared to normal adult monkey brains, indicating that Rab7-mediated transport was really disturbed. Growing evidences suggest that membrane-bound phosphoinositides regulate Rab-mediated endosome trafficking [61, 62], and the metabolism of phosphoinositides was affected by the disruption of insulin signaling [63–65]. Recent studies also showed that Rab activity is affected by insulin signaling and that PI3K inhibition causes upregulation of Rab5 [66, 67]. In the present study, we observed amyloid deposition in the pancreatic islets of all adult monkeys with DM. The remaining islet cells were severely degenerated and few in number, all characteristics of DM pathology in humans. These pancreatic pathologies suggest that insulin signaling also would be greatly impaired in the brains of DM-affected adult monkeys (Fig. 1A-D). Thus, although additional investigations are needed, impaired insulin signaling would exacerbate age-related endocytic disturbances via such alteration in the metabolism of phosphoinositides and/or Rab GTPases, inducing GAβ generation and ultimately resulting in enhanced Aβ pathology. It is reasonable idea because of the fact that insulin resistance is the core defect in DM [68]. In the brains of DM-affected adult monkeys, NEP levels were not affected (Fig. 6), suggesting that the enhanced SP deposition we observed is not due to disturbances in Aβ degradation by NEP.

In conclusion, we provide evidence that DM induces GAβ generation and accelerates Aβ pathology *in vivo* in cynomolgus monkey brains. Since the amino acid sequence of cynomolgus monkey Aβ corresponds completely with that of human Aβ, it is reasonable that the enhanced Aβ pathology we observed in monkeys with DM should also occur in humans with DM. Moreover, our present study showed that DM could also exacerbate endocytic disturbance. Although additional studies are needed to determine more precisely the mechanisms responsible for enhanced Aβ pathology in the brains of DM-affected monkeys, our findings suggest that DM may exacerbate age-dependent endocytic disturbance, leading to enhanced GAβ generation and Aβ fibril formation (Fig. 7). Importantly, several studies showed that Aβ impairs insulin signaling itself [69–71], and then it may lead to aggravate the insulin resistance-related AD pathology [11–13]. Thus enhanced Aβ pathology would contribute to DM-induced AD pathogenesis with such other mechanism (Fig. 7). Moreover, DM may also alter neuronal activity by exacerbating endocytic disturbance as we previously reported [46]. Hence, a reasonable therapeutic strategy to prevent the development of AD pathology is to treat or prevent DM.

Supporting Information

S1 ARRIVE Checklist. The ARRIVE Guidelines Checklist.
(PDF)

S1 Table. Clinical Background of monkeys analyzed in the present study.
(XLSX)

Acknowledgments

The authors thank Dr. Fumiko Ono for autopsy of cynomolgus monkeys. The authors also thank Dr. Naoto Oikawa for technical advice in dot blot analyses.

Author Contributions

Conceived and designed the experiments: NK. Performed the experiments: SO NK. Analyzed the data: SO NS YY KY NK. Contributed reagents/materials/analysis tools: NS YY. Wrote the paper: NK.

References

1. Armstrong RA (2009) The molecular biology of senile plaques and neurofibrillary tangles in Alzheimer's disease. Folia Neuropathol 47:289–299. PMID: 20054780
2. Mattson MP (2004) Pathways towards and away from Alzheimer's disease. Nature 430:631–639. PMID: 15295589
3. Hardy J, Selkoe DJ (2002) The amyloid hypothesis of Alzheimer's disease: progress and problems on the road to therapeutics. Science 297:353–356. PMID: 12130773
4. Goedert M, Sisodia SS, Price DL (1991) Neurofibrillary tangles and beta-amyloid deposits in Alzheimer's disease. Curr Opin Neurobiol 1:441–447. PMID: 1821689
5. Leibson CL, Rocca WA, Hanson VA, Cha R, Kokmen E, O'Brien PC, et al. (1997) Risk of dementia among persons with diabetes mellitus: a population-based cohort study. Am J Epidemiol 145:301–308. PMID: 9054233
6. Arvanitakis Z, Wilson RS, Bienias JL, Evans DA, Bennett DA (2004) Diabetes mellitus and risk of Alzheimer disease and decline in cognitive function. Arch Neurol 61:661–666. PMID: 15148141
7. Frisardi V, Solfrizzi V, Seripa D, Capurso C, Santamato A, et al. (2010) Metabolic-cognitive syndrome: a cross-talk between metabolic syndrome and Alzheimer's disease. Ageing Res Rev 9:399–417. doi: 10.1016/j.arr.2010.04.007 PMID: 20444434
8. Daviglus ML, Plassman BL, Pirzada A, Bell CC, Bowen PE, et al. (2011) Risk factors and preventive interventions for Alzheimer disease: state of the science. Arch Neurol 68:1185–1190. doi: 10.1001/archneurol.2011.100 PMID: 21555601
9. Crane PK, Walker R, Hubbard RA, Li G, Nathan DM, Zheng H, et al. (2013) Glucose levels and risk of dementia. N Engl J Med 369:540–548. doi: 10.1056/NEJMoa1215740 PMID: 23924004
10. Ott A, Stolk RP, van Harskamp F, Pols HAP, Hofman A, et al. (1999) Diabetes mellitus and the risk of dementia: the Rotterdam Study. Neurology 53:1937–1942. PMID: 10599761
11. De Felice FG, Ferreira ST (2014) Inflammation, defective insulin signaling, and mitochondrial dysfunction as common molecular denominators connecting type 2 diabetes to Alzheimer disease. Diabetes 63:2262–72. doi: 10.2337/db13-1954 PMID: 24931033
12. Salkovic-Petrisic M, Tribl F, Schmidt M, Hoyer S, Riederer P (2006) Alzheimer-like changes in protein kinase B and glycogen synthase kinase-3 in rat frontal cortex and hippocampus after damage to the insulin signalling pathway. J Neurochem 96:1005–15. PMID: 16412093
13. Baker LD, Cross DJ, Minoshima S, Belongia D, Watson GS, et al. (2010) Insulin resistance and Alzheimer-like reductions in regional cerebral glucose metabolism for cognitively normal adults with prediabetes or early type 2 diabetes. Arch Neurol 68:51–7. doi: 10.1001/archneurol.2010.225 PMID: 20837822
14. Ho L, Qin W, Pompl PN, Xiang Z, Wang J, et al. (2004) Diet-induced insulin resistance promotes amyloidosis in a transgenic mouse model of Alzheimer's disease. FASEB J 18:902–4. PMID: 15033922
15. Li Y, Duffy KB, Ottinger MA, Ray B, Bailey JA, et al. (2010) GLP-1 receptor stimulation reduces amyloid-beta peptide accumulation and cytotoxicity in cellular and animal models of Alzheimer's disease. J Alzheimers Dis 19:1205–19. doi: 10.3233/JAD-2010-1314 PMID: 20308787
16. Plaschke K, Kopitz J, Siegelin M, Schliebs R, Salkovic-Petrisic M, et al. (2010) Insulin-resistant brain state after intracerebroventricular streptozotocin injection exacerbates Alzheimer-like changes in Tg2576 AbetaPP-overexpressing mice. J Alzheimers Dis 19:691–704. doi: 10.3233/JAD-2010-1270 PMID: 20110613
17. Takeda S, Sato N, Uchio-Yamada K, Sawada K, Kunieda T, et al. (2010) Diabetes-accelerated memory dysfunction via cerebrovascular inflammation and Aβ deposition in an Alzheimer mouse model with diabetes. Proc Natl Acad Sci USA 107:7036–7041. doi: 10.1073/pnas.1000645107 PMID: 20231468

18. Bitela CL, Kasinathanb C, Kaswalab RH, Klein WL, Frederiksea PH (2012) Amyloid-β and Tau Pathology of Alzheimer's Disease Induced by Diabetes in a Rabbit Animal Model. Journal of Alzheimer's Disease 32:291–305. doi: 10.1111/tra.12264 PMID: 25615530

19. Currais A, Prior M, Lo D, Jolivalt C, Schubert D, et al. (2012) Diabetes exacerbates amyloid and neurovascular pathology in aging-accelerated mice. Aging Cell 11:1017–26. doi: 10.1111/acel.12002 PMID: 22938075

20. Maesako M, Uemura K, Kubota M, Kuzuya A, Sasaki K, et al. (2012) Environmental enrichment ameliorated high-fat diet-induced Aβ deposition and memory deficit in APP transgenic mice. Neurobiol Aging 33:1011.e11–23.

21. Son SM, Song H, Byun J, Park KS, Jang HC, et al. (2012) Accumulation of autophagosomes contributes to enhanced amyloidogenic APP processing under insulin-resistant conditions. Autophagy 8:1842–4. doi: 10.4161/auto.21861 PMID: 22931791

22. Yamamoto N, Matsubara T, Sobue K, Tanida M, Kasahara R, et al. (2012) Brain insulin resistance accelerates Aβ fibrillogenesis by inducing GM1 ganglioside clustering in the presynaptic membranes. J Neurochem 121:619–28. doi: 10.1111/j.1471-4159.2012.07668.x PMID: 22260232

23. Chen Y, Liang Z, Blanchard J, Dai CL, Sun S, et al. (2013) A non-transgenic mouse model (icv-STZ mouse) of Alzheimer's disease: similarities to and differences from the transgenic model (3xTg-AD mouse). Mol Neurobiol 47:711–25. doi: 10.1007/s12035-012-8375-5 PMID: 23150171

24. Yang Y, Wu Y, Zhang S, Song W (2013) High glucose promotes Aβ production by inhibiting APP degradation. PLoS One 8:e69824. doi: 10.1371/journal.pone.0069824 PMID: 23894546

25. Mehlaa J, Chauhanc BC, Chauhana NB (2014) Experimental Induction of Type 2 Diabetes in Aging-Accelerated Mice Triggered Alzheimer-Like Pathology and Memory Deficits. J Alzheimers Dis 39:145–162. doi: 10.3233/JAD-131238 PMID: 24121970

26. Nakamura S, Nakayama H, Goto N, Sakakibara I, Yosikawa Y (1998) Histopathological studies of senile plaques and cerebral amyloidosis in cynomolgus monkeys. J Med Primatol 27:244–252. PMID: 9926980

27. Oikawa N, Kimura N, Yanagisawa K (2010) Alzheimer-type tau pathology in advanced aged nonhuman primate brains harboring substantial amyloid deposition. Brain Res 1315:137–149. doi: 10.1016/j.brainres.2009.12.005 PMID: 20004650

28. Podlisny MB, Tolan DR, Selkoe DJ (1991) Homology of the amyloid beta protein precursor in monkey and human supports a primate model for beta amyloidosis in Alzheimer's disease. Am J Pathol 138:1423–1435. PMID: 1905108

29. Wagner JD, Cline JM, Shadoan MK, Bullock BC, Rankin SE, et al. (2001) Naturally occurring and experimental diabetes in cynomolgus monkeys: a comparison of carbohydrate and lipid metabolism and islet pathology. Toxicol Pathol 29: 142–148. PMID: 11215678

30. Wagner JE, Kavanagh K, Ward GM, Auerbach BJ, Harwood HJ Jr, et al. (2006) Old world nonhuman primate models of type 2 diabetes mellitus. ILAR J 47:259–271. PMID: 16804200

31. Bauer SA, Arndt TP, Leslie KE, Peral DL, Turner PV (2011) Obesity in rhesus and cynomolgus macaques: a comparative review of the condition and its implications for research. Comp Med 61:541–526.

32. Yanagisawa K, Odaka A, Suzuki N, Ihara Y (1995) GM1 ganglioside-bound amyloid beta-protein (A beta): a possible form of preamyloid in Alzheimer's disease. Nature Med 1:1062–1066. PMID: 7489364

33. Kimura N, Yanagisawa K (2007) Endosomal accumulation of GM1 ganglioside-bound amyloid beta-protein in neurons of aged monkey brains. Neuroreport 18:1669–1673. PMID: 17921865

34. Yuyama K, Yamamoto N, Yanagisawa K (2006) Chloroquine-induced endocytic pathway abnormalities: Cellular model of GM1 ganglioside-induced Abeta fibrillogenesis in Alzheimer's disease. FEBS Lett 580:6972–6976. PMID: 17161396

35. Tsuchida J, Yoshida T, Sankai T, Yasutomi Y (2008) Maternal behavior of laboratory-born, individually reared long-tailed macaques (Macaca fascicularis). J Am Assoc Lab Anim Sci 47:29–34. PMID: 18947167

36. Kimura N, Yanagisawa K, Terao K, Ono F, Sakakibara I, et al. (2005) Age-related changes of intracellular Abeta in cynomolgus monkey brains. Neuropathol Appl Neurobiol 31:170–180. PMID: 15771710

37. MacLaurin J, Chakrabartty A (1996) Membrane disruption by Alzheimer β-amyloid peptides mediated through specific binding to either phospholipids or gangliosides. Implications for neurotoxicity. J Biol Chem 271:26482–26489. PMID: 8900116

38. Choo-Smith LP, Garzon-Rodriguez W, Glabe CG, Surewicz WK (1997) Acceleration of amyloid fibril formation by specific binding of Abeta-(1–40) peptide to ganglioside-containing membrane vesicles. J Biol Chem 272:22987–22990. PMID: 9287293

39. Matsusaki K, Horikiri C (1999) Interactions of amyloid beta-peptide (1–40) with ganglioside-containing membranes. Biochemistry 38:4137–4142. PMID: 10194329

40. Kakio A, Nishimoto S, Yanagisawa K, Kozutsumi Y, Matsuzaki K (2002) Interactions of amyloid beta-protein with various gangliosides in raft-like membranes: importance of GM1 ganglioside-bound form as an endogenous seed for Alzheimer amyloid. Biochemistry 41:4385–7390. PMID: 11914085

41. Hayashi H, Kimura N, Yamaguchi H, Hasegawa K, Yokoseki T, et al. (2004) A seed for Alzheimer amyloid in the brain. J Neurosci 24:4894–4902. PMID: 15152051

42. Cataldo AM, Barnett JL, Pieroni C, Nixon RA (1997) Increased neuronal endocytosis and protease delivery to early endosomes in sporadic Alzheimer's disease: neuropathologic evidence for a mechanism of increased beta-amyloidogenesis. J Neurosci 17:6142–6151. PMID: 9236226

43. Cataldo AM, Peterhoff CM, Troncoso JC, Gomez-Isla T, Hyman BT, et al. (2000) Endocytic pathway abnormalities precede amyloid beta deposition in sporadic Alzheimer's disease and Down syndrome: differential effects of APOE genotype and presenilin mutations. Am J Pathol 157:277–286. PMID: 10880397

44. Cataldo AM, Petanceska S, Terio NB, Peterhoff CM, Durham R, et al. (2004) Abeta localization in abnormal endosomes: association with earliest Abeta elevations in AD a syndrome. Neurobiol Aging 25:1263–1272. PMID: 15465622

45. Kimura N, Inoue M, Okabayashi S, Ono F, Negishi T (2009) Dynein dysfunction induces endocytic pathology accompanied by an increase in Rab GTPases: a potential mechanism underlying age-dependent endocytic dysfunction. J Biol Chem 284:31291–31302. doi: 10.1074/jbc.M109.012625 PMID: 19758999

46. Kimura N, Okabayashi S, Ono F (2012) Dynein dysfunction disrupts intracellular vesicle trafficking bidirectionally and perturbs synaptic vesicle docking via endocytic disturbances a potential mechanism underlying age-dependent impairment of cognitive function. Am J Pathol 180:550–561. doi: 10.1016/j.ajpath.2011.10.037 PMID: 22182700

47. Kimura N, Tanemura K, Nakamura S, Takashima A, Ono F, et al. (2003) Age-related changes of Alzheimer's disease-associated proteins in cynomolgus monkey brains. Biochem Biophys Res Comm 310:303–311. PMID: 14521910

48. Schroer TA, Sheetz MP (1991) Functions of microtubule-based motors. Annu Rev Physiol 53:629–52. PMID: 2042975

49. Baptista FI, Pinto MJ, Elvas F, Almeida RD, Ambrósio AF (2013) Diabetes Alters KIF1A and KIF5B Motor Proteins in the Hippocampus. PLOS ONE 8:e65515. doi: 10.1371/journal.pone.0065515 PMID: 23776493

50. Nixon RA, Cataldo AM, Mathews PM (2000) The endosomal-lysosomal system of neurons in Alzheimer's disease pathogenesis: a review. Neurochem Res 25:1161–72. PMID: 11059790

51. Liu Y, Liu L, Lu S, Wang D, Liu X, et al. (2011) Impaired amyloid β-degrading enzymes in brain of streptozotocin-induced diabetic rat. J Endocrinol Invest 34:26–31. doi: 10.3275/6995 PMID: 20414044

52. Yuyama K, Yanagisawa K (2009) Late endocytic dysfunction as a putative cause of amyloid fibril formation in Alzheimer's disease. J Neurochem 109:1250–1260. doi: 10.1111/j.1471-4159.2009.06046.x PMID: 19317854

53. Cataldo AM, Barnett JL, Berman SA, Li J, Quarless S, et al. (1995) Gene expression and cellular content of cathepsin D in Alzheimer's disease brain: evidence for early up-regulation of the endosomal-lysosomal system. Neuron 14: 671–80. PMID: 7695914

54. Nixon RA, Wegiel J, Kumar A, Yu WH, Peterhoff C, et al. (2005) Extensive involvement of autophagy in Alzheimer disease: an immuno-electron microscopy study. J Neuropathol Exp Neurol 64: 113–22. PMID: 15751225

55. Boland B, Kumar A, Lee S, Platt FM, Wegiel J, et al. (2008) Autophagy induction and autophagosome clearance in neurons: relationship to autophagic pathology in Alzheimer's disease. J Neurosci 28: 6926–37. doi: 10.1523/JNEUROSCI.0800-08.2008 PMID: 18596167

56. Wolfe DM, Lee JH, Kumar A, Lee S, Orenstein SJ, et al. (2013) Autophagy failure in Alzheimer's disease and the role of defective lysosomal acidification. Eur J Neurosci 37: 1949–61. doi: 10.1111/ejn.12169 PMID: 23773064

57. Keilani S, Lun Y, Stevens AC, Williams HN, Sjoberg ER, et al. (2012) Lysosomal dysfunction in a mouse model of Sandhoff disease leads to accumulation of ganglioside-bound amyloid-β peptide. J Neurosci 32: 5223–36. doi: 10.1523/JNEUROSCI.4860-11.2012 PMID: 22496568

58. Tooze J, Hollinshead M, Ludwig T, Howell K, Hoflack B, et al. (1990) In exocrine pancreas, the basolateral endocytic pathway converges with the autophagic pathway immediately after the early endosome. J Cell Biol 111: 329–45. PMID: 2166050

59. Berg TO, Fengsrud M, Strømhaug PE, Berg T, Seglen PO (1998) Isolation and characterization of rat liver amphisomes. Evidence for fusion of autophagosomes with both early and late endosomes. J Biol Chem 273: 21883–92. PMID: 9705327

60. Gutierrez MG, Munafó DB, Berón W, Colombo MI (2004) Rab7 is required for the normal progression of the autophagic pathway in mammalian cells J Cell Sci 117: 2687–97. PMID: 15138286

61. Falkenburger BH, Jensen JB, Dickson EJ, Suh BC, Hille B (2010) Phosphoinositides: lipid regulators of membrane proteins. J Physiol 588: 3179–3185. doi: 10.1113/jphysiol.2010.192153 PMID: 20519312

62. Zhang X, Li X, Xu H (2012) Phosphoinositide isoforms determine compartment-specific ion channel activity. Proc Natl Acad Sci U S A 109: 11384–11389. doi: 10.1073/pnas.1202194109 PMID: 22733759

63. Natarajan V, Dyck PJ, Schmid HH (1981) Alterations of inositol lipid metabolism of rat sciatic nerve in streptozotocin-induced diabetes. J Neurochem 36: 413–9. PMID: 7463069

64. Thakker JK, DiMarchi R, MacDonald K, Caro JF (1989) Effect of Insulin and Insulin-like Growth Factors I and II on Phosphatidylinositol and Phosphatidylinositol 4,5-Bisphosphate Breakdown in Liver from Humans With and Without Type II Diabetes. J Biol Chem 264: 7169–7175. PMID: 2540178

65. Kamada T, McMillan DE, Otsuji S (1992) Changes in polyphosphoinositides and phosphatidic acid of erythrocyte membranes in diabetes. Diabetes Res Clin Pract 16: 85–90. PMID: 1318189

66. Huang J, Imamura T, Olefsky JM (2001) Insulin can regulate GLUT4 internalization by signaling to Rab5 and the motor protein dynein. Proc Natl Acad Sci USA 98:13084–13089. PMID: 11687655

67. Runyan CE, Liu Z, Schnaper HW (2012) Phosphatidylinositol 3-kinase and Rab5 GTPase inversely regulate the Smad anchor for receptor activation (SARA) protein independently of transforming growth factor-β1. J Biol Chem 287:35815–35824. doi: 10.1074/jbc.M112.380493 PMID: 22942286

68. Goldstein BJ (2002) Insulin resistance as the core defect in type 2 diabetes mellitus. Am J Cardiol 90:3G–10G. PMID: 12231073

69. Zhao WQ, De Felice FG, Fernandez S, Chen H, Lambert MP, et al. (2008) Amyloid beta oligomers induce impairment of neuronal insulin receptors. FASEB J 22:246–60. PMID: 17720802

70. De Felice FG, Vieira MN, Bomfim TR, Decker H, Velasco PT, et al. (2009) Protection of synapses against Alzheimer's-linked toxins: insulin signaling prevents the pathogenic binding of Abeta oligomers. Proc Natl Acad Sci U S A 106:1971–6. doi: 10.1073/pnas.0809158106 PMID: 19188609

71. Bomfim TR, Forny-Germano L, Sathler LB, Brito-Moreira J, Houzel JC, et al. (2012) An anti-diabetes agent protects the mouse brain from defective insulin signaling caused by Alzheimer's disease- associated Aβ oligomers. J Clin Invest 122:1339–53. doi: 10.1172/JCI57256 PMID: 22476196

Published February 13, 2015, doi:10.4049/jimmunol.1402027

Hydroxypropyl-β-Cyclodextrin Spikes Local Inflammation That Induces Th2 Cell and T Follicular Helper Cell Responses to the Coadministered Antigen

Motoyasu Onishi,*,†,‡,[1] Koji Ozasa,*,[1] Kouji Kobiyama,*,† Keiichi Ohata,*,† Mitsutaka Kitano,‡ Keiichi Taniguchi,‡ Tomoyuki Homma,‡ Masanori Kobayashi,‡ Akihiko Sato,‡ Yuko Katakai,§ Yasuhiro Yasutomi,¶ Edward Wijaya,‖ Yoshinobu Igarashi,# Noriyuki Nakatsu,# Wataru Ise,** Takeshi Inoue,** Hiroshi Yamada,# Alexis Vandenbon,‖ Daron M. Standley,‖ Tomohiro Kurosaki,**,†† Cevayir Coban,‡‡ Taiki Aoshi,*,† Etsushi Kuroda,*,† and Ken J. Ishii*,†

Cyclodextrins are commonly used as a safe excipient to enhance the solubility and bioavailability of hydrophobic pharmaceutical agents. Their efficacies and mechanisms as drug-delivery systems have been investigated for decades, but their immunological properties have not been examined. In this study, we reprofiled hydroxypropyl-β-cyclodextrin (HP-β-CD) as a vaccine adjuvant and found that it acts as a potent and unique adjuvant. HP-β-CD triggered the innate immune response at the injection site, was trapped by MARCO$^+$ macrophages, increased Ag uptake by dendritic cells, and facilitated the generation of T follicular helper cells in the draining lymph nodes. It significantly enhanced Ag-specific Th2 and IgG Ab responses as potently as did the conventional adjuvant, aluminum salt (alum), whereas its ability to induce Ag-specific IgE was less than that of alum. At the injection site, HP-β-CD induced the temporary release of host dsDNA, a damage-associated molecular pattern. DNase-treated mice, MyD88-deficient mice, and TBK1-deficient mice showed significantly reduced Ab responses after immunization with this adjuvant. Finally, we demonstrated that HP-β-CD–adjuvanted influenza hemagglutinin split vaccine protected against a lethal challenge with a clinically isolated pandemic H1N1 influenza virus, and the adjuvant effect of HP-β-CD was demonstrated in cynomolgus macaques. Our results suggest that HP-β-CD acts as a potent MyD88- and TBK1-dependent T follicular helper cell adjuvant and is readily applicable to various vaccines. *The Journal of Immunology*, **2015, 194: 000–000.**

The term "adjuvant" has its origin in the Latin "*adjuvare*" meaning "to help," because adjuvants enhance the effects of vaccines. Many substances can act as adjuvants, and their modes of action vary widely (1, 2). Recent studies showed that conventional adjuvants, such as alum, act via the "Ag-depot" mechanism, as well as induce multiple innate immune pathways, including the activation of inflammasomes, the production of PGE_2, and the release of damage-associated molecular patterns (DAMPs), such as DNA (3–5). In addition to enhancing the immunogenicity of vaccines, adjuvants can be responsible for their adverse effects, including local swelling, systemic fever, and a theoretical risk for autoimmunity (6). Even alum and MF59, widely used adjuvants for human vaccines, induce local and systemic adverse effects (6–8). Therefore, the high safety profile of an

*Laboratory of Adjuvant Innovation, National Institute of Biomedical Innovation, Osaka 567-0085, Japan; †Laboratory of Vaccine Science, Immunology Frontier Research Center, World Premier Institute, Osaka University, Osaka 565-0871, Japan; ‡Infectious Diseases, Medicinal Research Laboratories, Shionogi & Co., Ltd., Osaka 561-0825, Japan; §Corporation for the Production and Research of Laboratory Primates, Tsukuba, Ibaraki 305-0843, Japan; ¶Tsukuba Primate Research Center, National Institute of Biomedical Innovation, Tsukuba, Ibaraki 305-0843, Japan; ‖System Immunology Laboratory, Immunology Frontier Research Center, World Premier Institute, Osaka University, Osaka 565-0871, Japan; #Toxicogenomics Project, National Institute of Biomedical Innovation, Osaka 567-0085, Japan; **Laboratory of Lymphocyte Differentiation, Immunology Frontier Research Center, World Premier Institute, Osaka University, Osaka 565-0871, Japan; ††Laboratory for Lymphocyte Differentiation, RIKEN Center for Integrative Medical Sciences, Kanagawa 230-0045, Japan; and ‡‡Laboratory of Malaria Immunology, Immunology Frontier Research Center, World Premier Institute, Osaka University, Osaka 565-0871, Japan

[1]M.O. and K. Ozasa contributed equally to this work.

ORCID: 0000-0002-6728-3872 (K.J.I.).

Received for publication August 11, 2014. Accepted for publication December 3, 2014.

This work was supported by a Health and Labour Sciences Research Grant "Adjuvant Database Project" of the Japanese Ministry of Health, Labour and Welfare, the Regional Innovation Strategy Support Program, and Shionogi & Co., Ltd.

M.O., K. Ozasa, E.K., K.K., K. Ohata, W.I., T.I., T.K., T.A., and K.J.I. designed and performed the immunological research and analyzed the data. M. Kitano, K.T., T.H., M. Kobayashi, and A.S. designed and performed the murine influenza infectious model research and analyzed the data. E.W., Y.I., N.N., H.Y., A.V., D.M.S., and T.A. designed and performed the bioinformatics research and analyzed the data. E.K., K.K., Y.K., and Y.Y. designed and performed the cynomolgus macaque model research and analyzed the data. M.O., C.C., T.A., and K.J.I. wrote the manuscript.

The datasets presented in this article have been submitted to the National Center for Biotechnology Information's Gene Expression Omnibus (http://www.ncbi.nlm.nih.gov/geo/) under accession number GSE63332.

Address correspondence and reprint requests to Prof. Ken J. Ishii, Laboratory of Adjuvant Innovation, National Institute of Biomedical Innovation, 7-6-8 Asagi, Saito, Ibaraki-City, Osaka 567-0085, Japan or Immunology Frontier Research Center, Research Building 6F, Osaka University, 3-1 Yamada-oka, Suita-city, Osaka 565-0871, Japan. E-mail addresses: kenishii@nibio.go.jp or kenishii@biken.osaka-u.ac.jp

The online version of this article contains supplemental material.

Abbreviations used in this article: DAMP, damage-associated molecular pattern; DC, dendritic cell; GC, germinal center; GO, Gene Ontology; HA, hemagglutinin; HP-β-CD, hydroxypropyl-β-cyclodextrin; i.d., intradermal(ly); IFNAR, IFN-αβ receptor; KO, knockout; LN, lymph node; PA, presence/absence; SV, influenza trivalent split vaccine; Tfh, T follicular helper; TPRC, Tsukuba Primate Research Center; WT, wild-type.

www.jimmunol.org/cgi/doi/10.4049/jimmunol.1402027

adjuvant, based on scientific evidence, must be demonstrated before its application to clinical practice. One approach to identifying ideal adjuvants is the selection of candidate substances from among approved drugs or excipients with very high safety profiles.

Cyclodextrin is a bucket-shaped oligosaccharide derived from starch, with a hydrophobic cavity and hydrophilic exterior (9). Natural cyclodextrins contain six (α-CD), seven (β-CD), eight (γ-CD), or more (α-1,4)-linked α-*d*-glucopyranose units, and many chemically modified cyclodextrins have been developed, including hydroxypropyl-β-cyclodextrin (HP-β-CD) and sulfobutyl ether-β-cyclodextrin (9). Because of their molecular structure and shape, the cyclodextrins can form an inclusion complex with hydrophobic molecules, improving the solubility of hydrophobic drugs (9), stabilizing proteins (10), and controlling the release of drugs (11). For these reasons, cyclodextrins are widely used excipients for pharmaceutical agents (9). Recent studies showed another application of cyclodextrins in the treatment of Niemann–Pick type C1 disease; they reduced the lysosomal accumulation of cholesterol and glycosphingolipids (12). However, only a few studies have investigated the usefulness of cyclodextrins as vaccine adjuvants. Mucosal vaccination with dimethyl-β-cyclodextrin was shown to enhance the immunogenicity of anti-diphtheria and anti-tetanus toxoid total IgG titers in mice (13). Sulfolipo-cyclodextrin showed improved adjuvant activity when combined with squalene for use in cattle (14). The high safety profiles of the cyclodextrins and their potential adjuvant activities demonstrated in these studies are very valuable contributions to the development of new and safer adjuvants. However, research into cyclodextrins as vaccine adjuvants has not been thorough, and the mechanism of action of HP-β-CD as a vaccine adjuvant and its immunological characteristics are not well understood. In this study, we focused on HP-β-CD, one of the cyclodextrins most commonly used in pharmaceutical preparations, because its solubility is higher and its safety profile is better than those of other cyclodextrins (9). We demonstrate its activity as an immune adjuvant and the mechanisms involved. Our results indicate that HP-β-CD is a potent and promising T follicular help (Tfh) cell adjuvant for purified protein–based vaccines.

Materials and Methods

Ags and adjuvants

The following were used as Ags: extremely pure LPS-free OVA protein ([Seikagaku, Tokyo, Japan]; LPS contamination was <0.1 EU/mg, as measured with the *Limulus* Color KY test [Wako Pure Chemical Industries, Osaka, Japan], according to the manufacturer's protocol); influenza trivalent split vaccine (SV), containing influenza virus hemagglutinin (HA) surface Ags from three viral strains—A/California/7/2009 (H1N1), A/Victoria/210/2009 (H3N2), and B/Brisbane/60/2008; and monovalent SV, containing influenza virus HA surface Ag from New Caledonia/20/1999 (H1N1) (The Research Foundation for Microbial Diseases of Osaka University). SV was manufactured with egg-based technology (15). HP-β-CD (ISP Technologies, Assonet, MA), Good Manufacturing Practice grade K3 CpG-ODN (Gene Design, Osaka, Japan), and alum (InvivoGen, San Diego, CA) were used as adjuvants.

Mice and immunizations

Mice deficient for *Tlr1*, *Tlr2*, *Tlr3*, *Tlr4*, *Tlr5*, *Tlr6*, *Tlr7*, *Tlr9*, *Tlr7/9*, *Tlr2/4/9*, *Il1R*, *Il18R*, *St-2*, *Myd88*, *Tbk1*, *Irf3/7*, *Ifnar2*, *Asc*, and *Caspase 1* were generated and used for experiments previously (16). *Tlr*- or *Myd88*-knockout (KO) mice were purchased from Oriental BioService (Kyoto, Japan). *Irf3/7* double-KO mice were generated by cross-breeding with *Irf3*-KO mice and *Irf7*-KO mice (17). *Irf7*-KO mice were provided by the RIKEN BioResource Center through the National Bio-Resource Project of the Ministry of Education, Culture, Sports, Science and Technology (Ibaraki, Japan). $Bcl6^{flox/+}$ *Cd4*-cre ($Bcl6^{f/+}$) and $Bcl6^{flox/flox}$ *Cd4*-cre ($Bcl6^{f/f}$) mice were used for experiments previously (18). The other KO mice were housed and maintained at the National Institute of Biomedical Innovation. Wild-type (WT) C57BL/6 mice were purchased from CLEA Japan The mice were immunized s.c. twice with 100 μg OVA mixed with PBS (–), 30 μg K3 CpG-ODN, 1 mg alum, or 3–30% HP-β-CD [total volume: 200 μl in PBS (–)/mouse] on day 0 and day 10 after the first immunization. Sera were collected at 10, 17, 24, and 31 d after the first immunization. To evaluate the cellular immune responses, the mice were sacrificed and their spleens were collected 10 d after the second immunization. All experiments were performed under the appropriate laws and guidelines and after approval was obtained from the National Institute of Biomedical Innovation, the Animal Research Committee of the Research Institute for Microbial Diseases of Osaka University, and the Shionogi Animal Care and Use Committee.

Measurement of Ab titers

To measure the OVA- or HA-specific Ab titers, 96-well plates were coated with 100 μg/ml OVA solution or 1 μg/ml SV solution overnight at 4°C. The plates were washed and incubated for 1 h with blocking buffer [PBS (–) containing 1% BSA and 0.05% Tween 20]. After blocking, the plates were washed and incubated with 3-fold serially diluted serum for 2 h. To detect the bound Ab, the plates were washed and incubated for 1 h with HRP-conjugated anti-mouse total IgG, IgG1, or IgG2c Ab (Southern Biotech, Birmingham, AL) or anti-monkey total IgG Ab (Sigma, St. Louis, MO). After the plates were washed, TMB substrate solution was added to each well to initiate the color reaction. The reaction was stopped by the addition of 2 N H_2SO_4, and the OD was measured at a wavelength of 450 nm (OD_{450}). The Ab titer was defined as the highest serum dilution that yielded an $OD_{450} > OD_{450}$ of the negative-control serum. A DS Mouse IgE ELISA (OVA) kit (DS Pharma Biomedical, Osaka, Japan) was used to measure the concentration of anti-OVA IgE in the sera.

Evaluation of cellular immune responses

To evaluate the cellular immune responses, splenocytes (2×10^6 cell/well) were prepared and incubated with complete RPMI 1640 medium, containing 20 μg/ml OVA class I peptide, 20 μg/ml OVA class II peptide, or 20 μg/ml OVA Ag for 48 h at 37°C under 5% CO_2. The concentrations of IFN-γ, IL-5, and IL-13 in the cell culture supernatants were measured with the DuoSet ELISA Development System (R&D Systems, Minneapolis, MN).

Two-photon imaging of draining lymph nodes

OVA–Alexa Fluor 647 (Invitrogen, Carlsbad, CA) and HP-β-CD–FITC (Nanodex, Kanagawa, Japan) were used to visualize the distributions of Ag and HP-β-CD in the inguinal lymph nodes (LNs). The mice were injected intradermally (i.d.) at the tail base with 100 μg OVA–Alexa Fluor 647 mixed with 3% HP-β-CD–FITC. After 30 min, 10 μl rat anti-MARCO Ab (clone ED31; Serotec, Kidlington, U.K.) was injected i.d. The inguinal LNs were excised 30 min later and visualized with two-photon excitation microscopy (FV1000MPE; Olympus, Tokyo, Japan). The imaging data were analyzed with Volocity 3D Image Analysis Software (PerkinElmer, Waltham, MA). Pearson's correlation was calculated using Volocity colocalization analysis (PerkinElmer).

Evaluation of OVA uptake in draining LNs

To evaluate Ag uptake, we used DQ–OVA (Invitrogen), a self-quenching conjugate of OVA that displays bright green fluorescence upon proteolytic degradation. The mice were injected s.c. with PBS (–), 100 μg DQ–OVA, or 100 μg DQ–OVA mixed with 30% HP-β-CD (total volume, 200 μl/mouse), and the LNs were excised 24 h later. The LNs were cut and incubated in CO_2-independent medium (Life Technologies, CA) containing 1 mg/ml collagenase D and 2 μg/ml DNase I (both from Roche, Penzberg, Germany) for 30 min at 37°C. The cells (2×10^6 cell/sample) were prepared in FACS buffer [PBS (–) containing 1% FCS and 0.1% NaN_3]. FcγR was blocked with anti-mouse CD16/32 Ab (clone 93; eBioscience, San Diego, CA). Dead cells were stained with 7-aminoactinomycin D (eBioscience) and excluded from the analysis. To detect cells, Pacific Blue–conjugated anti-CD11c Ab (clone N418; BioLegend, San Diego, CA) was used. OVA uptake was assessed with a FACS LSR II flow cytometer (BD Biosciences, Franklin Lakes, NJ). The data were analyzed with FlowJo software (Tree Star, Ashland, OR).

Gene expression analysis

Mice ($n = 3$) were injected i.d. or i.p. with a total volume of 200 μl 30% HP-β-CD in PBS (–). The vehicle-control mice ($n = 3$) were injected with the same volume of PBS (–) without adjuvant. After 6 h, the inguinal LNs, liver, and spleen were removed and stored in RNAlater RNA Stabilization Reagent (Life Technologies). Each sample in RNAlater was homogenized in Buffer RLT (QIAGEN, Hilden, Germany) by adding a 5-mm-diameter zirconium bead (AS ONE, Osaka, Japan) and shaking with a Mixer Mill 300 (QIAGEN) at 20 Hz for 5 min. The total RNA was isolated and

purified from the sample homogenates with an RNeasy Mini Kit (QIAGEN), according to the manufacturer's instructions. The gene expression profiles were determined using the 3′ IVT Express Kit and the GeneChip Mouse Genome 430 2.0 Array (both from Affymetrix, Santa Clara, CA), according to the manufacturer's instructions. The expression values were normalized to the median value of each GeneChip readout. The resulting digital image files were preprocessed with the Affymetrix Microarray Suite version 5.0 algorithm (MAS5.0). The fold-change values were calculated as the ratio of the mean value for the treated samples/mean value for the vehicle-control samples. The presence/absence (PA) call in MAS5.0 was customized as described below. When the ratio was >1, the PA call was dependent on the treated samples, and when the ratio was ≤1, the call was dependent on the vehicle-control samples. Dominant calls (over half) were applied to a set of samples as the customized PA call, "P1" and "A0" (e.g., when the ratio < 1 and the PA call of control samples were "P," "P," and "A," the customized PA call of the set was "P1"). The MAS5.0 data and PA calls were analyzed with the Bioconductor Affy package for R (http://www.bioconductor.org). The *p* values indicating the significance of differentially expressed genes were calculated using a *t* test when comparing the normalized treated samples with the normalized vehicle-control samples. For our subsequent analysis, we only included probes for which the fold change between the control and the stimulated samples was >2. We excluded a probe when it was flagged "absent" (i.e., the PA call was "A0"). The fold change of the probes with PA call "A0" were replaced with 0. Finally, we used Z-score scaling for all of the probes to generate Fig. 3. All datasets were deposited in the National Center for Biotechnology Information's Gene Expression Omnibus (http://www.ncbi.nlm.nih.gov/geo/) under accession number GSE63332.

Evaluation of the generation of Tfh cells

Bcl6$^{f/+}$ or *Bcl6*$^{f/f}$ mice were immunized s.c. twice with 100 μg OVA mixed with 30% HP-β-CD [total volume: 200 μl in PBS (–)/mouse] on day 0 and 10 d after the first immunization. Inguinal LNs were collected 7 d after the second immunization. To detect Tfh cells, PE anti-mouse CD4 (clone RM4-5; BioLegend), allophycocyanin anti-mouse CD279 (PD-1; clone 29F.1A12; BioLegend), and FITC anti-mouse CD185 (CXCR5; clone L138D7; BioLegend) were used. FcγR was blocked with anti-mouse CD16/32 Ab (clone 93; eBioscience). Tfh cell generation was assessed with a BD LSRFortessa (BD Biosciences). The gating strategy is shown in Fig. 4A. The data were analyzed with FlowJo software (Tree Star).

Cytotoxicity assay

Cell viability after exposure to HP-β-CD was assessed in HEK293T cells (5×10^4 cell/well). Cytotoxicity was examined with a water-soluble tetrazolium salt-8 assay using the Cell Counting Kit-8 (Dojindo Molecular Technologies, Kumamoto, Japan), according to the manufacturer's instructions.

Measurement of dsDNA concentrations at injection sites

The mice were injected s.c. with 200 μl PBS (–) or 30% HP-β-CD. After 0.25, 0.5, 1, 3, 6, and 24 h, 400 μl PBS (–) was injected into the injection site, and the liquid in the pouch was collected. The liquid volume was adjusted to 1000 μl with PBS (–), and the acellular fraction was collected by centrifugation at 400 × *g* for 5 min at 4°C. The concentration of dsDNA in the acellular fraction was measured with a Qubit dsDNA HS Assay Kit (Invitrogen), according to the manufacturer's protocol.

Adjuvant activity of HP-β-CD in a murine influenza virus infection model

Mice were immunized s.c. twice with 3 μg SV mixed with PBS (–) or 3–30% HP-β-CD (total volume: 200 μl/mouse) on day 0 and 14 d after the first immunization. Sera were collected 14 and 21 d after the first immunization. Eight days after the second immunization, the mice were infected intranasally with 4×10^4 50% tissue culture infective dose ($TCID_{50}$) clinically isolated A/Osaka/129/2009 [A(H1N1)pdm09] influenza virus (19), which was obtained from Tetsuo Kase (Osaka Prefectural Institute of Public Health, Osaka, Japan). The body weights and survival rates of the mice were monitored for 14 d postinfection.

Adjuvant activity of HP-β-CD in a cynomolgus macaque model

Twelve male 3–5-y-old cynomolgus macaques (*Macaca fascicularis*) were obtained from the Tsukuba Primate Research Center (TPRC) of the National Institute of Biomedical Innovation and randomly assigned to four groups ($n = 3$). The macaques were immunized s.c. with saline or 5 μg New Caledonia/20/1999 (H1N1) SV mixed with PBS (–), 3% HP-β-CD, or 30% HP-β-CD (total volume: 500 μl/macaque) on day 0 and 14 d after the first immunization. Sera were collected at −2, 2, 4, 6, and 8 wk after the first immunization, and HA-specific IgG titers were measured with ELISAs. The experimental protocol was approved by the Animal Welfare and Animal Care Committee of the TPRC. All macaques were housed and handled by veterinarians in accordance with the Guidelines for Laboratory Animals of the TPRC.

Statistical analysis

The statistical significance of differences between groups was determined with the Student *t* test. The survival curves postinfection were compared with a Kaplan–Meier analysis (log-rank test and Wilcoxon test) using the statistical analysis software SAS for Windows (version 9.2; SAS Institute).

Results

HP-β-CD induces Th2 responses in a mouse model

To examine the activity of HP-β-CD as a vaccine adjuvant, we immunized C57BL/6 mice s.c. with LPS-free OVA, with or without different doses of HP-β-CD (3, 10, or 30%). Then the OVA-specific total IgG, IgG1, and IgG2c titers in the sera were determined with ELISAs. After the first immunization (day 10), the anti-OVA total IgG and IgG1 Ab titers were enhanced by all of the doses of HP-β-CD tested (Fig. 1A). In particular, the anti-OVA total IgG and IgG1 titers in the OVA/30% HP-β-CD group were significantly higher than those in the group treated with OVA alone. After boosting, the IgG2c response was also weakly induced, even by 3% HP-β-CD. Thus, all of the Ab titers in the OVA/30% HP-β-CD group were significantly increased on day 31 (21 d after boosting) relative to those in the group treated with OVA alone (Fig. 1A).

The T cell responses also were examined with cytokine ELISAs. Splenocytes from immunized mice were stimulated with OVA Ag or OVA-derived MHC class I– and MHC class II–restricted peptides. After 48 h, the production of IFN-γ, IL-5, and IL-13 was compared with that in splenocytes immunized with K3 CpG-ODN (a typical Th1-type adjuvant) or alum (a typical Th2-type adjuvant). Although HP-β-CD did not enhance IFN-γ production compared with K3 CpG-ODN, OVA/HP-β-CD immunization significantly increased IL-5 and IL-13 production, and the levels of these Th2-type cytokines were similar to those induced with alum (Fig. 1B). These results indicate that HP-β-CD elicits a Th2-type cell–mediated immune response when it is coadministered s.c. with OVA protein.

We then compared the IgE response induced by OVA/HP-β-CD immunization with that induced by alum. Alum is known to induce a high IgE response in animals and is commonly used to generate allergy models in mice (20). Mice were immunized s.c. twice with either OVA/30% HP-β-CD or OVA/alum. We also included K3 CpG-ODN, which is known to suppress Ag-specific IgE (21), as the negative control. Seven days after the booster immunization, the serum anti-OVA IgE concentrations were measured by ELISA. HP-β-CD induced a lower OVA-specific IgE response than did alum, whereas K3 induced virtually no IgE response (Fig. 1C). Interestingly, although HP-β-CD induced typical Th2-type cytokine (IL-5 and IL-13) responses (Fig. 1B), HP-β-CD also significantly increased the IgG2c titer, an indicator of the Th1-type immune response, in mice relative to that induced with OVA alone, although the levels of IgG2c were lower than those induced with K3. Taken together, these results suggest that HP-β-CD is a potent Th2-inducible adjuvant for OVA Ag, but it induces IgE less potently than does alum.

Additionally, we examined the adjuvanticity of HP-β-CD via several routes. When OVA/HP-β-CD was injected via the i.p. route, weaker adjuvanticity was observed compared with the s.c. route. With i.d. injection, Ab titer was elevated as seen with the s.c. route; however, skin inflammation was observed at the local injection site. No adjuvanticity of HP-β-CD was observed when

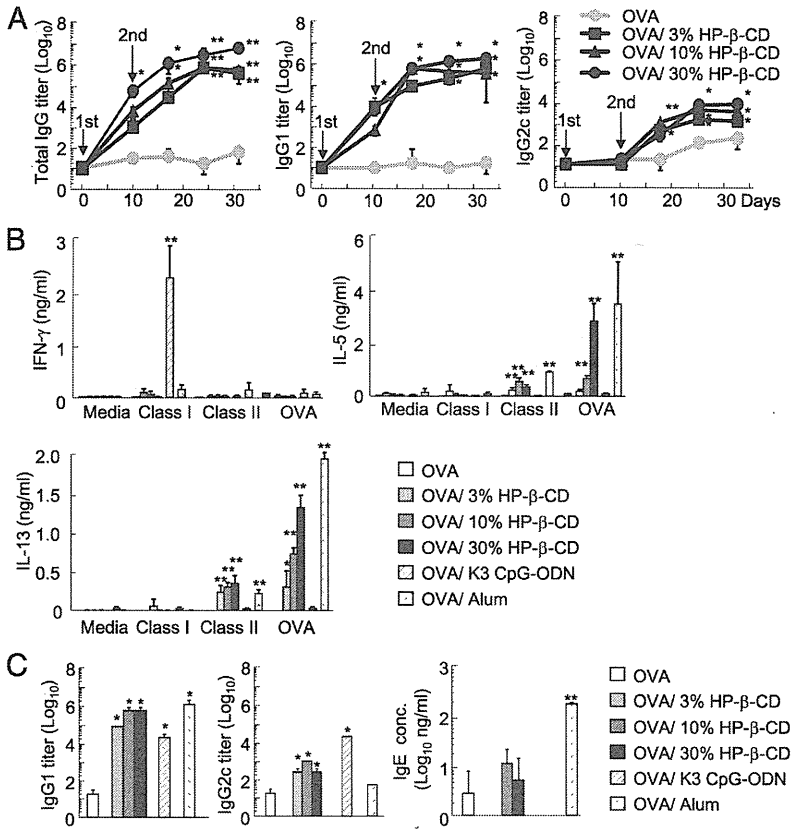

FIGURE 1. Humoral and cellular immune responses in mice after s.c. immunization with OVA/HP-β-CD. (**A**) Anti-OVA total IgG, IgG1, and IgG2c titers were measured with ELISAs at 10, 17, 24, and 31 d after the first immunization with OVA or OVA/HP-β-CD (each group, $n = 3$). (**B**) Splenocytes were collected from mice immunized with OVA, OVA/HP-β-CD, OVA/K3 CpG-ODN, or OVA/alum (each group, $n = 3$) at 10 d after the second immunization and stimulated with class I peptide ($OVA_{257-264}$), class II peptide ($OVA_{323-339}$), or OVA Ag. After incubation for 48 h, IFN-γ, IL-5, and IL-13 were measured in the supernatants with ELISAs. (**C**) IgG1 and IgG2c titers and IgE concentrations were compared 7 d after the second immunization (each group, $n = 3$). Data are representative of two independent experiments; error bars denote SD. $*p < 0.05$, $**p < 0.01$ versus OVA group on Student t test.

given via i.m. injection. These data suggest that the s.c. route results in adjuvanticity without inducing skin inflammation (data not shown).

HP-β-CD did not induce a systemic cytokine response

To further clarify the effects of HP-β-CD on the immune system, we investigated HP-β-CD–induced cytokine responses in naive mouse splenocytes in vitro. Splenocytes were stimulated with 200–5000 μg/ml (equivalent to 0.02–0.5%) HP-β-CD, and the cytokine concentrations in the supernatant were measured 24 h later using a multiplex assay. There was no significant increase in the cytokines (Supplemental Fig. 1A). Importantly, we could not stimulate the splenocytes with >0.5% HP-β-CD because higher concentrations appeared to cause immediate cell death in vitro. Therefore, we also investigated the cytokine responses in vivo. Mice were injected s.c. with 30% HP-β-CD, and their sera were collected 1, 3, and 8 h after injection. R848 also was injected into a separate group of mice as the positive control for systemic cytokine responses. Consistent with the in vitro result, we did not observe any detectable cytokine response in the sera at any time point examined when 30% HP-β-CD was injected, whereas injection of R848 induced significant responses in many cytokines (Supplemental Fig. 1B). These results indicate that HP-β-CD does not induce detectable levels of systemic cytokines either in vitro or in vivo (Supplemental Fig. 1).

Distribution of HP-β-CD and OVA in draining LNs

Without inducing proinflammatory responses in vitro and in vivo, HP-β-CD enhanced humoral responses after immunization. This result prompted us to investigate which cells incorporate HP-β-CD and play crucial roles in the adjuvanticity. We first used flow cytometry to investigate the cells in draining inguinal LNs after immunization; however, we could not identify the cells at a dose of 3% (the maximum dose of FITC-labeled HP-β-CD applicable to cells as a result of the HP-β-CD–FITC stock concentration limitation; data not shown). Therefore, we next performed two-photon microscopic analysis, which allows imaging of tissue to a substantial depth. We focused first on Siglec-1^+ (also called MOMA-1) macrophages, because inactivated influenza virus is captured by Siglec-1^+ macrophages, which induces humoral immune responses (22). The mice were injected with OVA–Alexa Fluor 647/3% HP-β-CD–FITC, and the explanted inguinal LNs were analyzed 1 h later. HP-β-CD was not incorporated into Siglec-1^+ macrophages (data not shown), but the majority of HP-β-CD was incorporated into macrophages carrying the macrophage receptor with collagenous structure ($MARCO^+$ macrophages) (23), and some HP-β-CD was found in the B cell follicle covering the $CD169^+$ subcapsular sinus macrophage area (Fig. 2A, Supplemental Video 1). When the distribution patterns of HP-β-CD and OVA were compared using Volocity's colocalization analysis, injected OVA was distributed more selectively in $MARCO^+$ macrophages than was HP-β-CD (Pearson correlation: HP-β-CD, +0.548, OVA, +0.756) (Fig. 2A, Supplemental Video 1), which is consistent with our recent observation (24). The recent study indicated that, although OVA and CpG (K3-SPG) were incorporated primarily into $MARCO^+$ macrophages, the macrophages are dispensable for inducing adaptive immune responses by CpG (K3-SPG). In addition, the study indicated the involvement of dendritic cells (DCs) in the adjuvanticity of CpG (K3-SPG). Based on these data, we next focused on DCs in LNs. To further clarify the uptake of Ag by DCs in LNs, mice were injected s.c. with DQ–OVA or DQ–OVA/30% HP-β-CD, and the uptake of OVA Ag by $CD11c^+$ cells was analyzed 24 h later using flow cytometry. Although the overall uptake was very small, OVA uptake by $CD11c^+$ DCs was enhanced significantly by HP-β-CD (Fig. 2B), suggesting that HP-β-CD acts as an Ag-delivery system

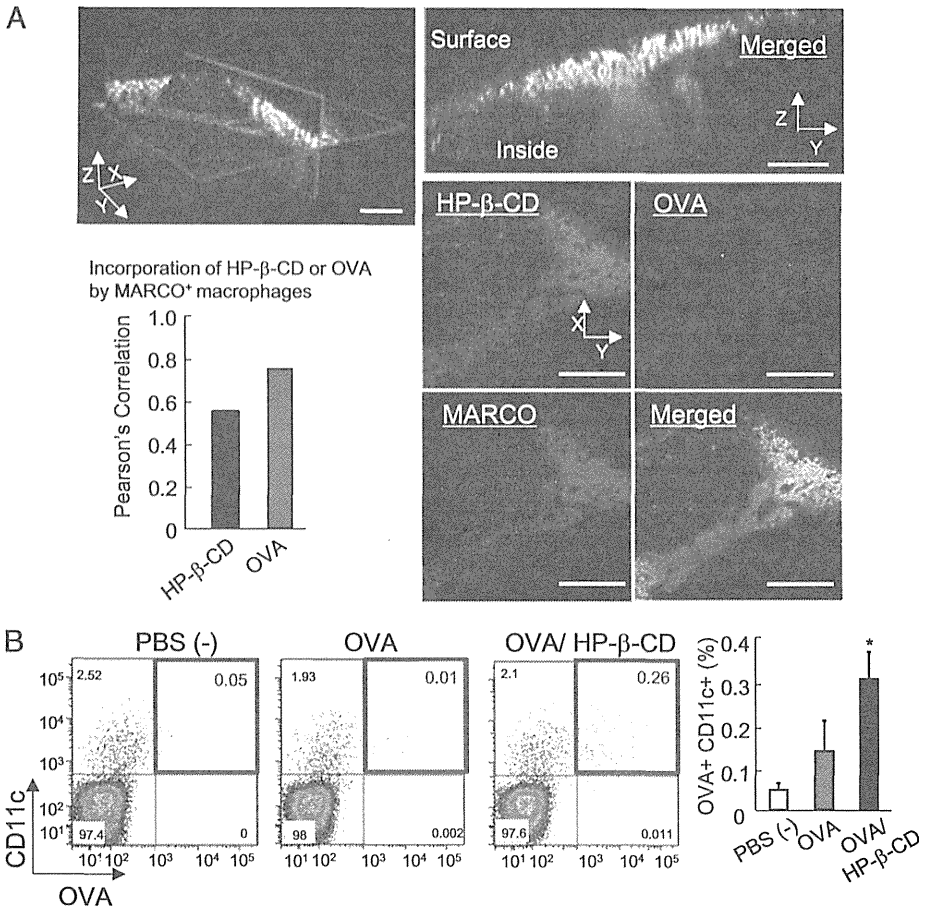

FIGURE 2. Distribution of HP-β-CD and OVA in LNs after injection. (**A**) Mice were injected i.d. with OVA–Alexa Fluor 647/HP-β-CD–FITC; anti-MARCO Ab was injected i.d. 30 min later. LNs were collected 30 min after the Ab injection (i.d.). Two-photon images of the LN. HP-β-CD (green), OVA (blue), MARCO$^+$ macrophages (red), and merged image. The distribution patterns of HP-β-CD and OVA were measured by Volocity's colocalization analysis. Scale bar, 100 μm. (**B**) Mice were injected s.c. with PBS (–), DQ–OVA, or DQ–OVA/30% HP-β-CD, and the LNs were collected after 24 h (n = 3). OVA uptake was assessed by flow cytometry. OVA$^+$CD11c$^+$ cells increased after DQ–OVA/30% HP-β-CD treatment. The bar graph shows the percentages of CD11c$^+$/OVA$^+$ cells. Data are representative of two independent experiments; error bars denote SD. *$p < 0.05$, versus PBS (–)–injected mice, Student t test.

to CD11c$^+$ cells. We also examined DC maturation after HP-β-CD injection in vivo but did not detect any upregulation of CD40 in the DCs (data not shown). It was difficult to investigate the function of MARCO$^+$ macrophages by flow cytometry (25). Collectively, we found a novel immunological mechanism of HP-β-CD that enhances Ag uptake by DCs.

HP-β-CD induced immune-related gene expression after local administration

To further clarify the mode of action of HP-β-CD, we performed a comprehensive mRNA GeneChip analysis. In our preliminary experiments, we noted that the adjuvant activity of HP-β-CD was weak after i.p. injection compared with that after s.c. or i.d. injection. Therefore, we compared gene expression in the draining inguinal LNs and other organs, such as the spleen and liver, 6 h after i.d. injection of HP-β-CD into the tail base (local) or i.p. injection (systemic). After local i.d. injection of HP-β-CD, the expression of substantial numbers of genes was induced >2-fold in the draining LNs, spleen, and liver (Fig. 3A). In contrast, i.p. injection of the same amount of HP-β-CD induced only limited changes in gene expression in the spleen and liver (Fig. 3A). We also performed a cluster analysis and categorized the induced genes into seven major groups (Supplemental Fig. 2A). Each group of genes was examined using Gene Ontology (GO) term analysis (Supplemental Fig. 2B). This analysis showed that HP-β-CD induced the expression of genes related to the innate immune response and the inflammatory response in the LNs, spleen, and liver after i.d. injection but not after i.p. injection (Fig. 3B, Supplemental Fig. 2, group 7), consistent with its route-dependent adjuvant activity. The GO term "defense response to virus" also was called in the group 1 cluster (Supplemental Fig. 2, group 1); correspondingly, the IFN response genes also were induced in the LNs after i.d. injection of HP-β-CD (Fig. 3C). The analysis of individual genes in Supplemental Fig. 2 revealed that those associated with the Th2-type immune response, including *Ptgs2* (26), *Nfil3* (27), and *Il33* (28), also were upregulated after i.d. injection of HP-β-CD (Fig. 3D). The induction of *Il1β* and *Myd88* genes (Fig. 3D) also suggested that inflammasomes could be activated in vivo by HP-β-CD. These data suggest that, despite the lack of detectable levels of cytokine production in the serum (Supplemental Fig. 1B), our GeneChip analysis demonstrated that HP-β-CD induced the expression of inflammatory and immune-related genes, including type I IFNs and *IL1β*, after i.d. injection but not after i.p. injection. These data are consistent with the route-dependent adjuvant activity of HP-β-CD.

Tfh cells are required for the adjuvanticity of HP-β-CD

Our GeneChip analysis found the induction of immune-related gene expression in LNs after HP-β-CD injection. A recent study indicated that Tfh cells, a Th cell subset present in germinal centers (GCs) in LNs, facilitate the generation of long-lived plasma cells and memory B cells, which are required for long-term Ab responses (29). To investigate the involvement of Tfh cells in the adjuvanticity of HP-β-CD, we evaluated their generation in LNs from *Bcl6*$^{f/+}$ or *Bcl6*$^{f/f}$ mice immunized with OVA or OVA/30% HP-β-CD. After the second immunization, the generation of Tfh cells was significantly increased by HP-β-CD in *Bcl6*$^{f/+}$ mice ($p < 0.05$), and it was significantly decreased in *Bcl6*$^{f/f}$ mice ($p < 0.0001$) (Fig. 4B). We also investigated the humoral responses between *Bcl6*$^{f/+}$ and *Bcl6*$^{f/f}$ mice after OVA/30% HP-β-CD

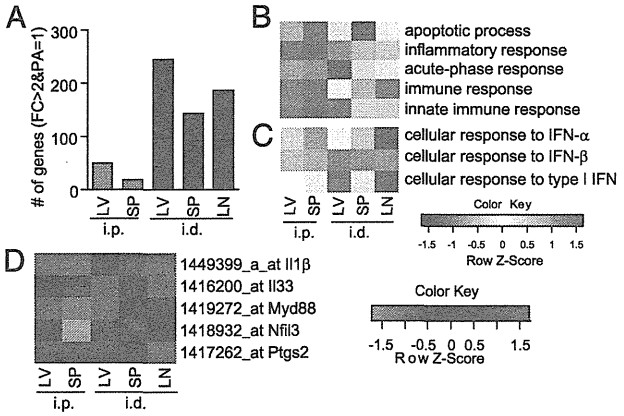

FIGURE 3. HP-β-CD induced substantial expression of immune-related genes after its local (i.d.) injection but not after its systemic (i.p.) injection. (**A**) The number of genes for which the fold change was >2 between HP-β-CD ($n = 3$) and PBS ($n = 3$) treatments and for which the customized PA call = 1 after 6 h when examined with a GeneChip array. (**B** and **C**) The expression levels of a selected immune-related set of genes categorized by GO terms are shown in the form of Z-scored fold-change values. The fold-change values were averaged and normalized using all of the genes in the corresponding GO term. The GO terms were derived and evoked from Supplemental Fig. 2. (**D**) Selected feature genes from Supplemental Fig. 2, presented by their Z-scores. The data are representative of two independent experiments with similar results. LV, liver; SP, spleen.

immunization. Consistent with the result of flow cytometric analysis, the anti-OVA IgG1 titer of *Bcl6*$^{f/f}$ mice was significantly lower than that of *Bcl6*$^{f/+}$ mice after the second immunization ($p < 0.01$) (Fig. 4C). However, the IgG1 titer of *Bcl6*$^{f/f}$ mice immunized with OVA/30% HP-β-CD was not decreased to the level of that of *Bcl6*$^{f/f}$ mice immunized with OVA alone, suggesting that the GC-independent pathway contributes, in part, to the induction of humoral responses after OVA/HP-β-CD immunization (30). These results suggested that the generation of Tfh cells is facilitated by the administration of HP-β-CD and that Tfh cells are required for the high adjuvanticity of HP-β-CD.

IL-21 secreted by Tfh cells can act in an autocrine manner to maintain Tfh cells at various stages of differentiation (29). Meanwhile, IL-21 was reported to prevent Ag-specific IgE response in mice (31). In this study, although HP-β-CD induced Th2 responses, it did not strongly induce an IgE response after immunization (Fig. 1C). To explain the weak IgE response after OVA/HP-β-CD immunization, we investigated IL-21 responses after stimulation of splenocytes from immunized *Bcl6*$^{f/+}$ mice; IL-21 responses were not observed from stimulated splenocytes (data not shown). Further research is necessary to explain why HP-β-CD does not induce strong IgE responses after immunization.

Inflammasome pathway does not contribute to the adjuvanticity of HP-β-CD

Our GeneChip analysis suggested that inflammasomes can be activated by HP-β-CD in vivo (Fig. 3B). Th2-inducible adjuvants, such as alum and silica, also were shown to activate inflammasomes in macrophages, whereas the role of inflammasomes in their adjuvant activity has been questioned (5). To clarify the immunological mechanisms and pathways essential for the adjuvant activity of HP-β-CD, we examined whether it activates inflammasomes in macrophages in vitro. Peritoneal macrophages were primed with LPS and stimulated with HP-β-CD 18 h later. Compared with alum, which induced high amounts of IL-1β, 5000 μg/ml (0.5%) HP-β-CD did not enhance the production of IL-1β by macrophages (data not shown). Because HP-β-CD is cytotoxic (see Fig. 5C), we could not examine the activation of inflammasomes at a higher concentration of HP-β-CD (equivalent to the maximum dose used in the immunization experiments performed in vivo) (Fig. 1). Therefore, we examined the humoral responses in *Asc*$^{-/-}$ mice and *Caspase 1*$^{-/-}$ mice, which are known to be deficient in inflammasome activation (32). The humoral response after s.c. immunization with OVA/HP-β-CD was not reduced in either gene-KO mouse strain (data not shown). Although these data do not exclude the possibility that the inflammasomes were activated in vivo after HP-β-CD injection, inflammasome activation was not required for the adjuvant activity of HP-β-CD.

MyD88 is involved in the adjuvant activity of HP-β-CD

To identify the pathway essential for the adjuvant activity of HP-β-CD, we focused on MyD88, a critical adapter protein of TLRs and the IL-1R superfamily, which are involved in the downstream activation of NF-κB and MAPK (33). TLRs are also key players in the activation of innate immunity and recognize various adjuvants and pathogen-associated molecular patterns. Mice lacking *Myd88* were immunized s.c. twice with OVA/HP-β-CD. After the second immunization, the anti-OVA IgG and IgG1 titers of *Myd88*$^{-/-}$ mice were significantly lower than those of *Myd88*$^{+/-}$ mice (Fig. 5A). Interestingly, *Myd88*$^{-/-}$ mice immunized with OVA/HP-β-CD showed significantly higher total IgG and IgG1 titers than did WT mice immunized with OVA alone. These results suggest that both MyD88-dependent and -independent signaling pathways are involved in the adjuvant activity of HP-β-CD. A TLR-screening assay was performed in vitro to identify the upstream receptor of MyD88-dependent signaling. The TLR4-signaling pathway was activated slightly by HP-β-CD (Supplemental Fig. 3A), so we examined whether TLR4 is involved in the adjuvant activity of HP-β-CD in vivo; however, the humoral response was not reduced in *Tlr4*$^{-/-}$ mice (Supplemental Fig. 3B). We then investigated other TLRs or members of the IL-1R superfamily by s.c. immunizing other *Tlrs*, *Il1R*, *Il18R*, and *St-2* KO mice. ST-2 is a receptor that forms a complex with IL-1R accessory protein; it

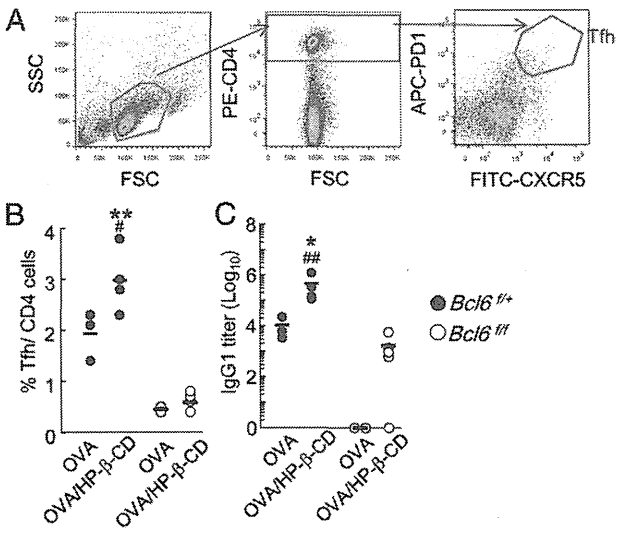

FIGURE 4. Tfh cell development and humoral responses after OVA/HP-β-CD immunization. *Bcl6*$^{f/+}$ or *Bcl6*$^{f/f}$ mice were immunized s.c. with OVA or OVA/30% HP-β-CD ($n = 2$–5). (**A**) Flow cytometric analysis was performed to assess the generation of Tfh cells. (**B**) Seven days after the second immunization, Tfh cell generation was measured. (**C**) Anti-OVA IgG1 titers were measured with ELISAs 7 d after the second immunization. Error bars denote SD. $^{\#}p < 0.05$, $^{\#\#}p < 0.01$ versus *Bcl6*$^{f/+}$ mice immunized with OVA alone, $^{*}p < 0.01$, $^{**}p < 0.0001$ versus *Bcl6*$^{f/f}$ mice immunized with OVA/30% HP-β-CD, Student *t* test.

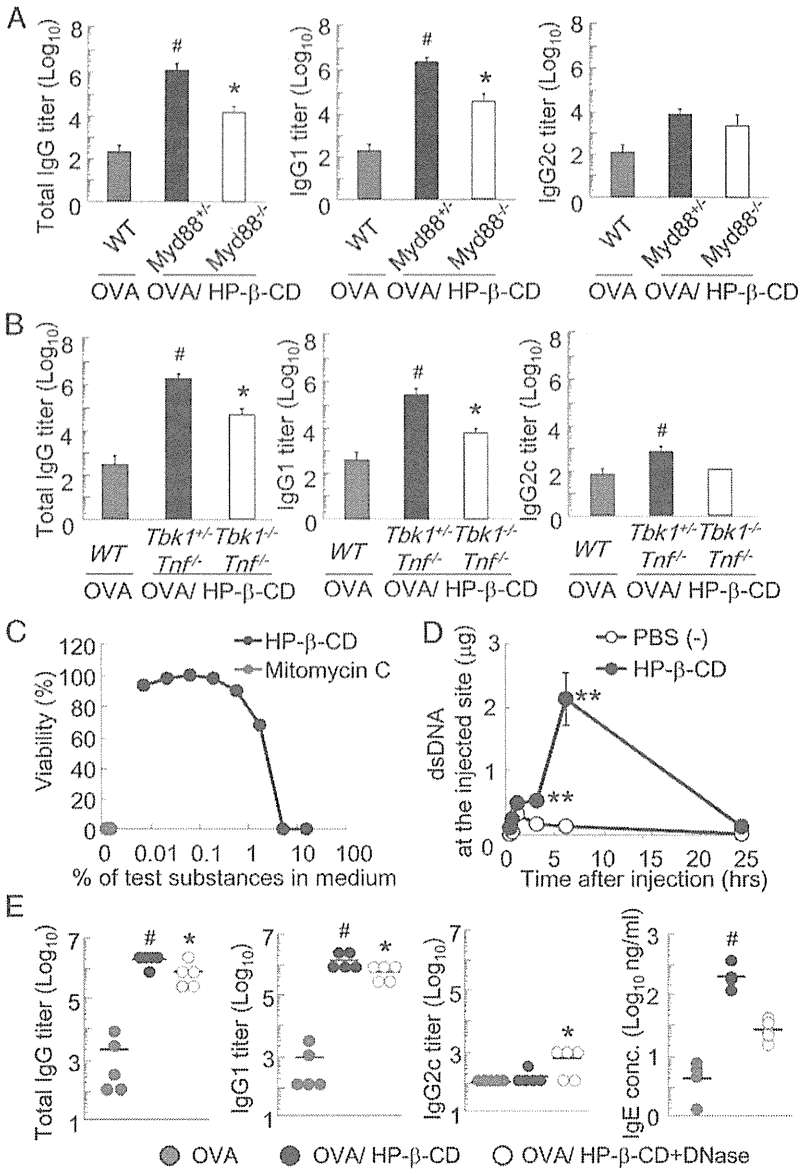

FIGURE 5. Evaluation of the involvement of MyD88 and TBK1 in the adjuvant activity of HP-β-CD. Mice lacking MyD88 (**A**) or TBK1 (**B**) were s.c. immunized twice with OVA/ HP-β-CD (n = 6-10). Anti-OVA total IgG, IgG1, and IgG2c titers were measured with ELISAs 7 d after the second immunization. $^{\#}p < 0.05$ versus KO mice,$^{*}p < 0.05$ versus WT mice immunized with OVA alone on Student t test. (**C**) The cytotoxicity of HP-β-CD for HEK293T cells was assessed with a WST-8 assay after incubation for 24 h (n = 3). (**D**) Concentration of dsDNA in the acellular fraction of the liquid pouch at the injection site was measured 0.25, 0.5, 1, 3, 6, and 24 h after s.c. injection (n = 3). $^{**}p < 0.01$ on Student t test. (**E**) OVA/ HP-β-CD (n = 5) immunization (s.c.) was performed with or without 2 mg of DNase I (Roche). Anti-OVA total IgG, IgG1, and IgG2c titers and IgE concentrations were measured 7 d after the second immunization. $^{\#}p < 0.05$ versus OVA/HP-β-CD+DNase group, $^{*}p < 0.05$ versus OVA group on Student t test. Error bars denote SD.

can bind IL-33 directly, and it mediates Th2 responses (28). All of the examined KO mice, including TLR7/9 double-deficient and TLR2/4/9 triple-deficient mice, showed anti-OVA total IgG titers that were similar to those of WT mice 7 d after the booster immunization (Supplemental Fig. 3B). Notably, after stimulation with HP-β-CD, no significant increases in proinflammatory cytokines, chemokines, or growth factors were detected in vitro (Supplemental Fig. 1A). Taken together, these results suggest that HP-β-CD itself may activate TLR4 in vitro. However, in vivo, the adjuvant activity of HP-β-CD is independent of any single TLR, TLR7/9, TLR2/4/9, or the IL-1R superfamily, although the adjuvant activity of HP-β-CD is partially dependent on MyD88 signaling.

HP-β-CD induces dsDNA release, and TBK1contributes to its adjuvanticity

The results described above suggest that a MyD88-independent pathway is involved in the adjuvant activity of HP-β-CD. Our GeneChip analysis suggested that HP-β-CD induces type I IFN–related gene responses in the draining LNs (Fig. 3). Therefore, we examined the involvement of IFN-αβ receptor (IFNAR), IRF3/7, and TBK1 by using mice in which the representative gene is knocked out. *Tbk1*$^{-/-}$ mice on a TNF-deficient (*Tnf*$^{-/-}$) background were used because *Tbk1*$^{-/-}$ mice die in utero, and this lethal effect can be rescued in the absence of TNF (34). The humoral responses in IFNAR2 and IRF3/7 double-KO mice were similar to those in WT mice (data not shown). However, the anti-OVA IgG titer in *Tbk1*$^{-/-}$ mice was significantly lower than that in *Tnf*$^{-/-}$ mice (Fig. 5B), suggesting that TBK1 also contributes to the adjuvant activity of HP-β-CD but that its activity is independent of type I IFN responses.

We showed that alum induces the release of dsDNA from host cells, resulting in TBK1/IRF3-dependent, but IFNAR2-independent, Th2 responses (16). The results described above indicating TBK1 involvement prompted us to examine the release of dsDNA from host cells after the local injection of HP-β-CD. We first examined the cytotoxicity of HP-β-CD against HEK293T cells in vitro. HP-β-CD started killing HEK293 cells at a concentration of 0.5%; at 1.5%, almost all of the cells were killed. However, the overall cytotoxicity of HP-β-CD was 1,000,000 times lower than that of mitomycin C, which damages cells by DNA cross-linking (35) (Fig. 5C). In an in vivo study, we observed the adjuvant activity of 3% HP-β-CD in mice (Fig. 1A). These data suggest that HP-β-CD

potentially causes the release of dsDNA from host cells in vivo, similar to alum. To examine this possibility, we tested whether HP-β-CD induced the release of host DNA in vivo. HP-β-CD was injected s.c. into mice, and the concentration of host DNA at the injection site, which formed a liquid pouch under the skin, was measured. Increasing amounts of dsDNA, triggered by HP-β-CD, were detected until 6 h, after which they decreased and returned to background levels at 24 h after injection (Fig. 5D). This result suggests that HP-β-CD triggers temporary host dsDNA release at its injection site. Furthermore, DNase I treatment at the time of immunization significantly reduced the total IgG, IgG1, and IgE titers but enhanced the IgG2c response (Fig. 5E). This result strongly suggests that HP-β-CD triggers dsDNA release, which acts as a DAMP, triggering a signal through the TBK1-dependent pathway and resulting in an enhanced Th2-type immune response. However, at the same time, HP-β-CD induces a MyD88-dependent response, which may modulate the IgE response upregulated by the dsDNA/TBK1 axis. Further study is required to identify the critical upstream/downstream pathways of MyD88 and TBK1 induced by the local administration of HP-β-CD.

HP-β-CD shows potent adjuvanticity with SV

Although HP-β-CD temporarily triggered the release of dsDNA (Fig. 5D), it did not elicit strong IgE responses (Fig. 1C), and it induced almost no systemic cytokine responses in mice (Supplemental Fig. 1B). This suggests that HP-β-CD is a suitable adjuvant for a current split influenza vaccine. Most influenza vaccines are used to immunize healthy individuals, so minimizing the toxicity of the vaccine is an absolute requirement for the adjuvant. We evaluated the adjuvant activity of HP-β-CD using an influenza SV immunization model in mice and macaques. Mice were immunized s.c. twice with SV only or with SV/3–30% HP-β-CD, and their total IgG titers were measured with an ELISA. After the booster immunization, the anti-HA total IgG titer was significantly enhanced by all doses of HP-β-CD tested (Fig. 6A). After the immunized mice were challenged with a lethal dose of A/Osaka/129/2009 [A(H1N1)pdm09] influenza virus, their body weights and survival rates were determined for 14 d. The survival and body weight parameters of the SV/HP-β-CD–immunized groups were significantly better than were those of the group immunized with SV only (Fig. 6B, 6C).

To further estimate the adjuvant activity of HP-β-CD in humans, cynomolgus macaques were immunized s.c. twice with saline, SV, SV/3% HP-β-CD, or SV/30% HP-β-CD, and their anti-HA IgG titers were evaluated every 2 wk. The anti-HA IgG titers of all macaques in the SV/30% HP-β-CD group were increased 2 wk after the first immunization (Fig. 7A). A boosting effect of HP-β-CD also was observed in this group (Fig. 7A). The anti-HA IgG titers of the SV group varied greatly among individuals (Fig. 7A). When we compared the geometric mean titer of the anti-HA IgG titers of the SV/30% HP-β-CD group and the SV group, the anti-HA IgG titer of the SV/30% HP-β-CD group was 3-fold higher than that of the SV group 2 wk after the first immunization, and it was 2-fold higher than that of the SV group 6 wk after the second immunization (Fig. 7B). Unlike the results for mice, the anti-HA IgG titers in the SV/3% HP-β-CD group were not better than those in the SV group (Fig. 7). These results demonstrate that 30% HP-β-CD displays adjuvant activity with the influenza SV vaccine in both mice and cynomolgus macaques.

Discussion

In addition to their efficacy, one of the most important characteristics of vaccine adjuvants is their safety, because many vaccines are intended for use in healthy individuals. HP-β-CD has been used safely as an excipient for pharmaceutical agents for decades (9). However, no extensive immunological characterization of

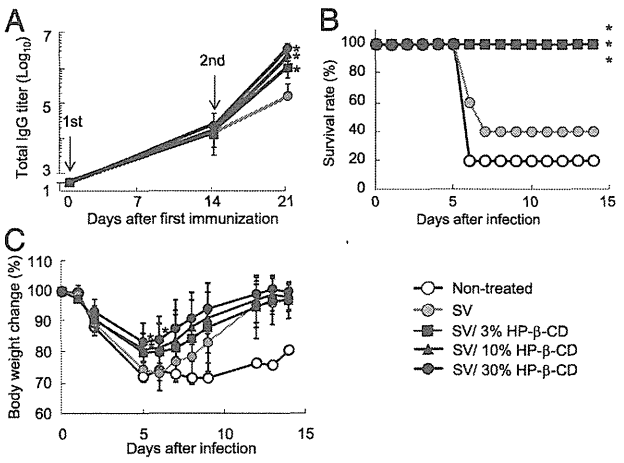

FIGURE 6. Efficacy of SV/HP-β-CD against influenza virus infection in mice. (**A**) Mice were immunized s.c. twice with SV or SV/HP-β-CD on day 0 and 14 d after the first immunization, and the total anti-HA IgG titers were measured with ELISA at 14 and 21 d (n = 5). (**B** and **C**) Mice were challenged with 4 × 10^4 50% $TCID_{50}$ A/Osaka/129/2009 [A(H1N1) pdm09] influenza virus 21 d after the first immunization. Their body weight changes and survivals were monitored. Data are representative of two independent experiments. Error bars denote SD. *$p < 0.05$, versus SV group, Student t test (A and C) or Kaplan–Meier analysis (log-rank test and Wilcoxon test) (B).

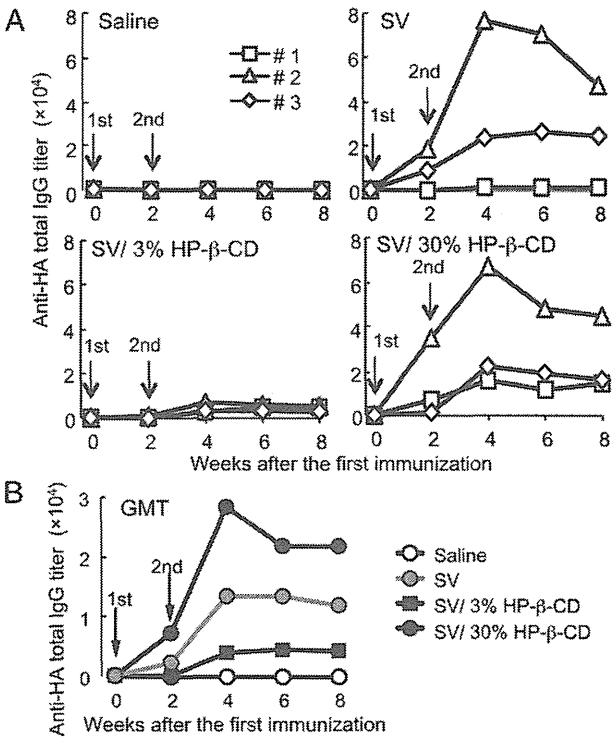

FIGURE 7. Immunogenicity of SV/HP-β-CD in cynomolgus macaques. Cynomolgus macaques were immunized twice with saline, SV, SV/3% HP-β-CD, or SV/30% HP-β-CD on day 0 and 14 d after the first immunization (n = 3). The sera were collected every 2 wk, and anti-HA total IgG titers were measured using ELISA. (**A**) Individual results. (**B**) Geometric mean titers (GMT) of the groups (n = 3).

cyclodextrins as adjuvants has been conducted, so the molecular and cellular mechanisms of their actions are largely unknown. Our characterization of HP-β-CD as a vaccine adjuvant revealed that it induces unique Th2 responses, enhancing Ag-specific IgG titers, including IgG1 and IgG2c titers, by s.c. injection. Furthermore, the adjuvanticity is largely dependent on Tfh cells. Unlike alum, a commonly used adjuvant for many human vaccines throughout the world, HP-β-CD induced little IgE production (Fig. 1A, 1C). A T cell analysis clearly indicated that HP-β-CD preferentially activates Th2 cells over Th1 cells (Fig. 1B). Traditionally, it has been considered that the Th2 and IgE responses are sequential, but our current data indicate that Th2 induction does not always induce strong IgE production. The ability of an adjuvant to induce IgE may be a crucial risk factor affecting the allergenic potential of vaccines. Therefore, HP-β-CD may be a safer adjuvant than alum because it entails less risk for inducing potentially allergic IgE responses. Injection of HP-β-CD obviously induced some acute inflammatory, type I IFN–related and Th2-associated gene responses in LNs. However, no systemic proinflammatory cytokine responses were observed after its injection into mice (Supplemental Fig. 1B), suggesting that the gene expression induced in LNs does not induce systemic proinflammatory cytokine responses, which can be detrimental to the host. Without inducing systemic proinflammatory cytokine responses, HP-β-CD exhibited enough adjuvanticity to improve the immunogenicity and protective efficacy of SV in mice and cynomolgus macaques. Hence, we conclude that HP-β-CD is a well-balanced adjuvant possessing high adjuvant activity and little risk for inducing allergic potential IgE responses and systemic inflammation.

The activation of immune responses in LNs is a major event to establish adaptive immunity (29). Our cellular analysis found enhanced Ag uptake by DCs and generation of Tfh cells in LNs after OVA/HP-β-CD injection (Figs. 2B, 4B). In addition, Tfh cells were required for the high adjuvanticity of HP-β-CD (Fig. 4C). DCs provide signals that upregulate CXCR5 and downregulate CCR7 on naive $CD4^+$ T cells, allowing them to migrate to B cell follicles and, consequently, facilitate the generation of Tfh cells (29). Tfh cells are recognized as the key player required for the formation of GCs and the generation of long-lived serological memory (30). Therefore, these results explained why humoral responses were enhanced and maintained by HP-β-CD.

The biological effects of HP-β-CD are reported to include the binding and sequestration of plasma membrane cholesterol and, consequently, the dispersal of lipid rafts, which include lipids and associated plasma membrane–spanning proteins, such as sphingolipids (36). Such treatments are considered to affect the lateral diffusion, aggregation, and function of receptor complexes (37). Bioactive lipids, such as ceramides and sphingosine 1-phosphate, are known to regulate inflammation in cells and to activate several signaling pathways (38). Therefore, it is reasonable to infer that HP-β-CD activates the innate immune response and exerts its adjuvant activity by modifying these lipid-dependent biological processes. Methyl-β-cyclodextrin is reported to disperse lipid rafts, thereby stimulating MyD88-dependent NF-κB activation in immature B cells, and it partially stimulates the TLR4-signaling pathway in vitro (39). In this study, the results of an in vitro TLR-screening assay supported those findings (Supplemental Fig. 3A). However, analysis of gene-KO mice indicated that MyD88, but not TLR4, contributes, in part, to the adjuvant activity of HP-β-CD (Supplemental Fig. 3B), suggesting that signaling pathways other than TLR pathways, such as lipid raft dispersal/MyD88/NF-κB activation, contribute to the MyD88-dependent mechanism underlying the adjuvant activity of HP-β-CD (Supplemental Fig. 4). This is an important issue for future research.

We also demonstrated that TBK1 contributes, in part, to the adjuvant activity of HP-β-CD (Fig. 5B). HP-β-CD causes the release of several factors, including lipids and dsDNA, that may function as DAMPs to activate the innate immune response. In this study, HP-β-CD induced the temporary release of dsDNA at its injection site. These facts strongly suggest that the adjuvant activity of HP-β-CD is also mediated by host-derived factors, such as DAMPs. Therefore, it is reasonable that the adjuvant activity of HP-β-CD was not diminished in single *Myd88*- or *Tbk1*-deficient mice. Our findings indicate that the activation of several signaling pathways as a result of HP-β-CD injection contributes to its adjuvant activity (Supplemental Fig. 4).

It is important to exploit the safety profile of HP-β-CD for the development of adjuvanted vaccines. Vaccination is the primary strategy used to prevent influenza infection. The efficacy of influenza vaccines in young and healthy adults is estimated to be 70–90%, but it is <17–53% in the elderly (40). The use of an adjuvant to improve the efficacy of a vaccine has been investigated, but minimizing adjuvant toxicity remains one of the major challenges in adjuvant research (41). To exploit the safety profile of HP-β-CD, we evaluated the combined effects of HP-β-CD and SV and demonstrated that HP-β-CD enhanced the protective efficacy of SV against influenza virus infection in mice (Fig. 6). Its adjuvant activity also was examined in cynomolgus macaques (Fig. 7). In the macaque model, the anti-HA IgG titers were not strongly elevated in any of macaques in the SV group. In contrast, immunization with SV/30% HP-β-CD strongly enhanced the anti-HA IgG titers of all of the macaques in the group. To improve the efficacy of SV, it is important to overcome the poor immunogenicity and enhance the humoral responses of weak responders with an adjuvant. In contrast to the results with s.c. injection, we did not find adjuvanticity for HP-β-CD via the i.m. route. The i.m. route is a major route for human vaccines; however, all seasonal influenza SVs are injected s.c. in Japan. Outside of Japan, some influenza vaccines, such as Fluvax (42) and VAXIGRIP (43), are acceptable to inject s.c. Therefore, the lack of adjuvanticity of HP-β-CD via i.m. injection is not a major concern. Collectively, our results suggest that HP-β-CD is a promising adjuvant for enhancing the immunogenicity of s.c. SV injections in humans.

This study has important implications, demonstrating that HP-β-CD is safe and can be used effectively as an adjuvant for SV in humans. It also contributes novel immunological findings that advance cyclodextrin research and promote the innovation of a rationally designed safer adjuvant.

Acknowledgments

We thank Tetsuo Kase for providing the A/Osaka/129/2009 virus. We also thank Akiko Okabe, Mariko Nakamura, Yuko Fujita, Aki Konishi, Kousaku Murase, and Yasunari Haseda for excellent technical assistance with animal husbandry and genotyping, as well as the members of K.J.I.'s and C.C.'s laboratories for valuable comments and help.

Disclosures

The authors have no financial conflicts of interest.

References

1. Dey, A. K., and I. K. Srivastava. 2011. Novel adjuvants and delivery systems for enhancing immune responses induced by immunogens. *Expert Rev. Vaccines* 10: 227–251.
2. Reed, S. G., M. T. Orr, and C. B. Fox. 2013. Key roles of adjuvants in modern vaccines. *Nat. Med.* 19: 1597–1608.
3. Marrack, P., A. S. McKee, and M. W. Munks. 2009. Towards an understanding of the adjuvant action of aluminium. *Nat. Rev. Immunol.* 9: 287–293.
4. Desmet, C. J., and K. J. Ishii. 2012. Nucleic acid sensing at the interface between innate and adaptive immunity in vaccination. *Nat. Rev. Immunol.* 12: 479–491.

5. Kuroda, E., K. J. Ishii, S. Uematsu, K. Ohata, C. Coban, S. Akira, K. Aritake, Y. Urade, and Y. Morimoto. 2011. Silica crystals and aluminum salts regulate the production of prostaglandin in macrophages via NALP3 inflammasome-independent mechanisms. *Immunity* 34: 514–526.
6. Batista-Duharte, A., E. B. Lindblad, and E. Oviedo-Orta. 2011. Progress in understanding adjuvant immunotoxicity mechanisms. *Toxicol. Lett.* 203: 97–105.
7. Hwang, S. M., H. L. Kim, K. W. Min, M. Kim, J. S. Lim, J. M. Choi, B. C. Chun, M. J. Kim, S. M. Lee, S. Y. Kim, and H. H. Jeon. 2012. Comparison of the adverse events associated with MF59-adjuvanted and non-adjuvanted H1N1 vaccines in healthy young male Korean soldiers. *Jpn. J. Infect. Dis.* 65: 193–197.
8. Frey, S., G. Poland, S. Percell, and A. Podda. 2003. Comparison of the safety, tolerability, and immunogenicity of a MF59-adjuvanted influenza vaccine and a non-adjuvanted influenza vaccine in non-elderly adults. *Vaccine* 21: 4234–4237.
9. Brewster, M. E., and T. Loftsson. 2007. Cyclodextrins as pharmaceutical solubilizers. *Adv. Drug Deliv. Rev.* 59: 645–666.
10. Serno, T., R. Geidobler, and G. Winter. 2011. Protein stabilization by cyclodextrins in the liquid and dried state. *Adv. Drug Deliv. Rev.* 63: 1086–1106.
11. Vyas, A, S. Saraf, and S. Saraf. 2008. Cyclodextrin based novel drug delivery systems. *J. Incl. Phenom. Macrocycl. Chem.* 62: 23–42.
12. Rosenbaum, A. I., and F. R. Maxfield. 2011. Niemann-Pick type C disease: molecular mechanisms and potential therapeutic approaches. *J. Neurochem.* 116: 789–795.
13. Alpar, H. O., J. E. Eyles, E. D. Williamson, and S. Somavarapu. 2001. Intranasal vaccination against plague, tetanus and diphtheria. *Adv. Drug Deliv. Rev.* 51: 173–201.
14. Romera, S. A., L. A. Hilgers, M. Puntel, P. I. Zamorano, V. L. Alcon, M. J. Dus Santos, J. Blanco Viera, M. V. Borca, and A. M. Sadir. 2000. Adjuvant effects of sulfolipo-cyclodextrin in a squalane-in-water and water-in-mineral oil emulsions for BHV-1 vaccines in cattle. *Vaccine* 19: 132–141.
15. Tanimoto, T., R. Nakatsu, I. Fuke, T. Ishikawa, M. Ishibashi, K. Yamanishi, M. Takahashi, and S. Tamura. 2005. Estimation of the neuraminidase content of influenza viruses and split-product vaccines by immunochromatography. *Vaccine* 23: 4598–4609.
16. Marichal, T., K. Ohata, D. Bedoret, C. Mesnil, C. Sabatel, K. Kobiyama, P. Lekeux, C. Coban, S. Akira, K. J. Ishii, et al. 2011. DNA released from dying host cells mediates aluminum adjuvant activity. *Nat. Med.* 17: 996–1002.
17. Honda, K., H. Yanai, H. Negishi, M. Asagiri, M. Sato, T. Mizutani, N. Shimada, Y. Ohba, A. Takaoka, N. Yoshida, and T. Taniguchi. 2005. IRF-7 is the master regulator of type-I interferon-dependent immune responses. *Nature* 434: 772–777.
18. Ise, W., T. Inoue, J. B. McLachlan, K. Kometani, M. Kubo, T. Okada, and T. Kurosaki. 2014. Memory B cells contribute to rapid Bcl6 expression by memory follicular helper T cells. *Proc. Natl. Acad. Sci. USA* 111: 11792–11797.
19. Kitano, M., M. Kodama, Y. Itoh, T. Kanazu, M. Kobayashi, R. Yoshida, and A. Sato. 2013. Efficacy of repeated intravenous injection of peramivir against influenza A (H1N1) 2009 virus infection in immunosuppressed mice. *Antimicrob. Agents Chemother.* 57: 2286–2294.
20. Nordvall, S. L., O. Grimmer, T. Karlsson, and B. Björkstén. 1982. Characterization of the mouse and rat IgE antibody responses to timothy pollen by means of crossed radioimmunoelectrophoresis. *Allergy* 37: 259–264.
21. Kline, J. N., T. J. Waldschmidt, T. R. Businga, J. E. Lemish, J. V. Weinstock, P. S. Thorne, and A. M. Krieg. 1998. Modulation of airway inflammation by CpG oligodeoxynucleotides in a murine model of asthma. *J. Immunol.* 160: 2555–2559.
22. Gonzalez, S. F., V. Lukacs-Kornek, M. P. Kuligowski, L. A. Pitcher, S. E. Degn, Y. A. Kim, M. J. Cloninger, L. Martinez-Pomares, S. Gordon, S. J. Turley, and M. C. Carroll. 2010. Capture of influenza by medullary dendritic cells via SIGN-R1 is essential for humoral immunity in draining lymph nodes. *Nat. Immunol.* 11: 427–434.
23. Areschoug, T., and S. Gordon. 2009. Scavenger receptors: role in innate immunity and microbial pathogenesis. *Cell. Microbiol.* 11: 1160–1169.
24. Kobiyama, K., T. Aoshi, H. Narita, E. Kuroda, M. Hayashi, K. Tetsutani, S. Koyama, S. Mochizuki, K. Sakurai, Y. Katakai, et al. 2014. Nonagonistic Dectin-1 ligand transforms CpG into a multitask nanoparticulate TLR9 agonist. *Proc. Natl. Acad. Sci. USA* 111: 3086–3091.
25. Gray, E. E., and J. G. Cyster. 2012. Lymph node macrophages. *J. Innate Immun.* 4: 424–436.
26. Kuroda, E., and U. Yamashita. 2003. Mechanisms of enhanced macrophage-mediated prostaglandin E2 production and its suppressive role in Th1 activation in Th2-dominant BALB/c mice. *J. Immunol.* 170: 757–764.
27. Kashiwada, M., S. L. Cassel, J. D. Colgan, and P. B. Rothman. 2011. NFIL3/E4BP4 controls type 2 T helper cell cytokine expression. *EMBO J.* 30: 2071–2082.
28. Schmitz, J., A. Owyang, E. Oldham, Y. Song, E. Murphy, T. K. McClanahan, G. Zurawski, M. Moshrefi, J. Qin, X. Li, et al. 2005. IL-33, an interleukin-1-like cytokine that signals via the IL-1 receptor-related protein ST2 and induces T helper type 2-associated cytokines. *Immunity* 23: 479–490.
29. Ma, C. S., E. K. Deenick, M. Batten, and S. G. Tangye. 2012. The origins, function, and regulation of T follicular helper cells. *J. Exp. Med.* 209: 1241–1253.
30. Kaji, T., A. Ishige, M. Hikida, J. Taka, A. Hijikata, M. Kubo, T. Nagashima, Y. Takahashi, T. Kurosaki, M. Okada, et al. 2012. Distinct cellular pathways select germline-encoded and somatically mutated antibodies into immunological memory. *J. Exp. Med.* 209: 2079–2097.
31. Suto, A., H. Nakajima, K. Hirose, K. Suzuki, S. Kagami, Y. Seto, A. Hoshimoto, Y. Saito, D. C. Foster, and I. Iwamoto. 2002. Interleukin 21 prevents antigen-induced IgE production by inhibiting germ line C(epsilon) transcription of IL-4-stimulated B cells. *Blood* 100: 4565–4573.
32. Eisenbarth, S. C., O. R. Colegio, W. O'Connor, F. S. Sutterwala, and R. A. Flavell. 2008. Crucial role for the Nalp3 inflammasome in the immunostimulatory properties of aluminium adjuvants. *Nature* 453: 1122–1126.
33. Akira, S., K. Takeda, and T. Kaisho. 2001. Toll-like receptors: critical proteins linking innate and acquired immunity. *Nat. Immunol.* 2: 675–680.
34. Ishii, K. J., T. Kawagoe, S. Koyama, K. Matsui, H. Kumar, T. Kawai, S. Uematsu, O. Takeuchi, F. Takeshita, C. Coban, and S. Akira. 2008. TANK-binding kinase-1 delineates innate and adaptive immune responses to DNA vaccines. *Nature* 451: 725–729.
35. Tomasz, M., and Y. Palom. 1997. The mitomycin bioreductive antitumor agents: cross-linking and alkylation of DNA as the molecular basis of their activity. *Pharmacol. Ther.* 76: 73–87.
36. Zidovetzki, R., and I. Levitan. 2007. Use of cyclodextrins to manipulate plasma membrane cholesterol content: evidence, misconceptions and control strategies. *Biochim. Biophys. Acta* 1768: 1311–1324.
37. Pralle, A., P. Keller, E. L. Florin, K. Simons, and J. K. Hörber. 2000. Sphingolipid-cholesterol rafts diffuse as small entities in the plasma membrane of mammalian cells. *J. Cell Biol.* 148: 997–1008.
38. Gomez-Muñoz, A., P. Gangoiti, L. Arana, A. Ouro, I. G. Rivera, M. Ordoñez, and M. Trueba. 2013. New insights on the role of ceramide 1-phosphate in inflammation. *Biochim. Biophys. Acta* 1831: 1060–1066.
39. Flemming, J. A., K. H. Perkins, L. Luus, A. R. Ferguson, and R. B. Corley. 2004. Disruption of membrane cholesterol stimulates MyD88-dependent NF-kappaB activation in immature B cells. *Cell. Immunol.* 229: 68–77.
40. Goodwin, K., C. Viboud, and L. Simonsen. 2006. Antibody response to influenza vaccination in the elderly: a quantitative review. *Vaccine* 24: 1159–1169.
41. Aguilar, J. C., and E. G. Rodríguez. 2007. Vaccine adjuvants revisited. *Vaccine* 25: 3752–3762.
42. CSL Biotherapies (New Zealand) Ltd. Fluvax product datasheet. Available at: http://www.medsafe.govt.nz/profs/datasheet/f/Fluvaxinj.pdf. Accessed: July 2, 2014.
43. Sanofi pasteur. Vaxigrip product datasheet. Available at: http://products.sanofi.com.au/vaccines/VAXIGRIP_NZ_PI_2013-03.pdf. Accessed: July 2, 2014.

OPEN

Nanogel-based pneumococcal surface protein A nasal vaccine induces microRNA-associated Th17 cell responses with neutralizing antibodies against *Streptococcus pneumoniae* in macaques

Y Fukuyama[1], Y Yuki[1,2], Y Katakai[3], N Harada[4], H Takahashi[5], S Takeda[5], M Mejima[1], S Joo[1], S Kurokawa[1], S Sawada[5], H Shibata[6], EJ Park[1], K Fujihashi[7], DE Briles[8], Y Yasutomi[6], H Tsukada[4], K Akiyoshi[5] and H Kiyono[1,2]

We previously established a nanosized nasal vaccine delivery system by using a cationic cholesteryl group-bearing pullulan nanogel (cCHP nanogel), which is a universal protein-based antigen-delivery vehicle for adjuvant-free nasal vaccination. In the present study, we examined the central nervous system safety and efficacy of nasal vaccination with our developed cCHP nanogel containing pneumococcal surface protein A (PspA-nanogel) against pneumococcal infection in nonhuman primates. When [^{18}F]-labeled PspA-nanogel was nasally administered to a rhesus macaque (*Macaca mulatta*), longer-term retention of PspA was noted in the nasal cavity when compared with administration of PspA alone. Of importance, no deposition of [^{18}F]-PspA was seen in the olfactory bulbs or brain. Nasal PspA-nanogel vaccination effectively induced PspA-specific serum IgG with protective activity and mucosal secretory IgA (SIgA) Ab responses in cynomolgus macaques (*Macaca fascicularis*). Nasal PspA-nanogel-induced immune responses were mediated through T-helper (Th) 2 and Th17 cytokine responses concomitantly with marked increases in the levels of miR-181a and miR-326 in the serum and respiratory tract tissues, respectively, of the macaques. These results demonstrate that nasal PspA-nanogel vaccination is a safe and effective strategy for the development of a nasal vaccine for the prevention of pneumonia in humans.

INTRODUCTION

Streptococcus pneumoniae is a major cause of bacterial infections throughout the world and is involved in the induction of a wide variety of infectious diseases, including otitis media, pneumonia, bacteremia, and meningitis in children and adults. This organism is usually a commensal bacterium in the upper respiratory tract of humans. Currently, four pneumococcal vaccines, 7-, 10- and 13-valent polysaccharide conjugate vaccines (PCV7, 10, 13) for children and a 23-valent pneumococcal polysaccharide vaccine (PPV23) for adults, have been developed for public use and are delivered by intramuscular injection.[1–3] However, as the conjugate vaccine does not protect against other capsular types, it provides little or no protection against total colonization with pneumococci.[4,5] The extensive carriage by other pneumococcal capsular types has led to strain replacement in disease with strains of non-conjugate vaccine capsular types.[6,7]

[1]Division of Mucosal Immunology, The Institute of Medical Science, The University of Tokyo, Minato-ku, Tokyo, Japan. [2]International Research and Development Center for Mucosal Vaccine, The Institute of Medical Science, The University of Tokyo, Minato-ku, Tokyo, Japan. [3]Corporation for Production and Research of Laboratory Primates, Tsukuba, Ibaraki, Japan. [4]PET Center, Central Research Laboratory, Hamamatsu Photonics K.K., Hamamatsu, Shizuoka, Japan. [5]Department of Polymer Chemistry, Kyoto University Graduate School of Engineering, Nishikyo-ku, Kyoto, Japan. [6]Tsukuba Primate Research Center, National Institute of Biomedical Innovation, Tsukuba, Ibaraki, Japan. [7]Departments of Pediatric Dentistry and Microbiology, The Immunobiology Vaccine Center, The University of Alabama at Birmingham, Birmingham, Alabama, USA and [8]Department of Microbiology, The University of Alabama at Birmingham, Birmingham, Alabama, USA. Correspondence: Y Yuki or H Kiyono (yukiy@ims.u-tokyo.ac.jp or kiyono@ims.u-tokyo.ac.jp)

Received 1 June 2014; accepted 2 January 2015; advance online publication 11 February 2015. doi:10.1038/mi.2015.5

The development of effective protein-based vaccines, which have the potential to provide better coverage for all strains, and to protect against colonization with all strains requires a thorough understanding of the roles and relative contributions to pathogenesis of the various putative virulence proteins. The pneumococcal surface protein A (PspA) is a well-known highly immunogenic surface protein of *S. pneumoniae* and is considered to be a promising vaccine candidate.[8,9] It is present on virtually all strains of pneumococci, and PspA-based vaccines against *S. pneumoniae* induce cross-reactive Abs in mice[10,11] and humans.[12] Moreover, PspA-specific mucosal and serum Abs responses are induced, and these responses are mediated by both Th1- and Th2-type cytokine production by $CD4^+$ T cells in infant mice via maternal immunization,[13] as well as in aged mice.[14] These findings indicate that PspA is a potent antigen for the development of effective pneumococcal vaccines not only in adults but also in children and the elderly.

S. pneumoniae commonly colonizes the nasal cavity, which can be protected by mucosal IgA.[15–17] Nasal vaccination induces effective mucosal immune responses in the respiratory tract, where initial bacterial and viral infections commonly occur; it could therefore be an effective immunization strategy for delivering protection from pneumococcal infection. However, most subunit type vaccines are poor immunogens for the induction of antigen-specific immune response in both systemic and mucosal immune compartments when nasally administered. Thus, the co-administration of biologically active mucosal adjuvants (e.g., cholera toxin and heat-labile toxin) or a better delivery system is needed to overcome the disadvantages of nasal antigen exposure. However, there are currently no safe nasal adjuvants or delivery systems, as evaluated by safety pharmacology studies, such as absorption, distribution, metabolism, and excretion in preclinical studies.

To overcome these concerns, we recently developed an effective vaccine delivery system with a self-assembled nanosized hydrogel (nanogel), which is composed of a cationic type of cholesteryl group-bearing pullulan (cCHP).[18] This cCHP nanogel efficiently delivers an antigen to epithelial cells in the nasal cavity, as well as to dendritic cells (DCs) under the basement membrane, and induces antigen-specific immune responses as an adjuvant-free vaccine.[19,20] Furthermore, a radioisotope counting assay showed that nasally administered cCHP nanogel carrying the [^{111}In]-labeled non-toxic subunit of botulinum neurotoxin does not accumulate in parts of the central nervous system (CNS) in mice.[19] In our separate study, we demonstrated that a nasally administered PspA-nanogel vaccine is safe and induces strong antigen-specific systemic and mucosal Ab immune responses, which can protect mice from invasive challenge with *S. pneumoniae*.[21]

MicroRNAs (miRNAs) have emerged as important regulators of many biological processes associated with the immune system, including the function of both innate and adaptive immune responses.[22–24] Accumulating evidence indicates that miRNA has an essential role in eliciting immune responses. For example, mice with T lymphocytes in which the endoribonuclease dicer, which is critical for miRNA biogenesis, has been conditionally knocked out show impaired thymic development and diminished Th-cell differentiation.[25,26] Dicer deficiency in B cells also prevents B-cell development.[27] These findings indicate the critical functions of miRNAs in the biology of the cells that constitute the immune system, such as in the development and differentiation of lymphocytes. Therefore, it is important to identify the miRNA biomarkers that engage in both mucosal and systemic antibody responses induced by nasal immunization with PspA-nanogel. Together, better understanding of the precise engagement of miRNAs in mediating humoral and protective immunity will be beneficial for the development of effective mucosal vaccines.

Before pursuing a clinical trial of a PspA-nanogel-based vaccine, we designed experiments to assess its safety for the CNS and its immunological efficacy, including immunologically relevant miRNA expression, and to demonstrate its safety and efficacy in nonhuman primates.

RESULTS

[^{18}F]-PspA-nanogel is retained for a long time in the nasal cavity but is not deposited in the olfactory bulbs or brain after nasal administration in macaques

We initially confirmed the physicochemical characterization of PspA-nanogel vaccine used in this study (**Supplementary Figure S1** online), and then investigated the retention of nasal PspA-nanogel in the nasal cavity and its accumulation in the olfactory bulbs and CNS in nonhuman primates by using three naive rhesus macaques. Because the results were nearly identical for the three macaques, we show the results for only one of the macaques in **Figure 1** (primate #1). The macaque's head was placed in the positron emission tomography (PET) scanner system and real-time imaging was performed for 6 h. To confirm the exact position of the cerebrum, we performed a magnetic resonance imaging (MRI) scan and then superimposed the PET images onto the MRI images. The real-time PET images clearly showed that nasally administered [^{18}F]-PspA-nanogel was effectively delivered to the nasal mucosa and retained in the nasal tissues for up to 6 h (**Figure 1a,c**). In contrast, most of the free form of [^{18}F]-PspA without a nanogel had disappeared from the nasal cavity by 3 h after nasal administration (**Figure 1a**). Furthermore, no deposition of [^{18}F]-PspA was detected in the cerebrum or olfactory bulbs of macaques, even 6 h after nasal administration (**Figure 1b**). These results show that PspA-nanogel is a CNS-safe and effective nasal vaccine delivery system in nonhuman primates.

Nasal vaccination with PspA-nanogel induces mucosal and systemic Ab responses in macaques

We next examined whether the nasal PspA-nanogel vaccine induced PspA-specific immune responses in cynomolgus macaques (primates #2-#9). One week after the final immunization, PspA-specific serum IgG Ab responses were significantly increased in macaques nasally immunized with 25 μg of PspA-nanogel when compared with macaques immunized with PspA alone or PBS only (**Figure 2a**). Examination of the longevity of PspA-nanogel-induced serum antigen-specific IgG

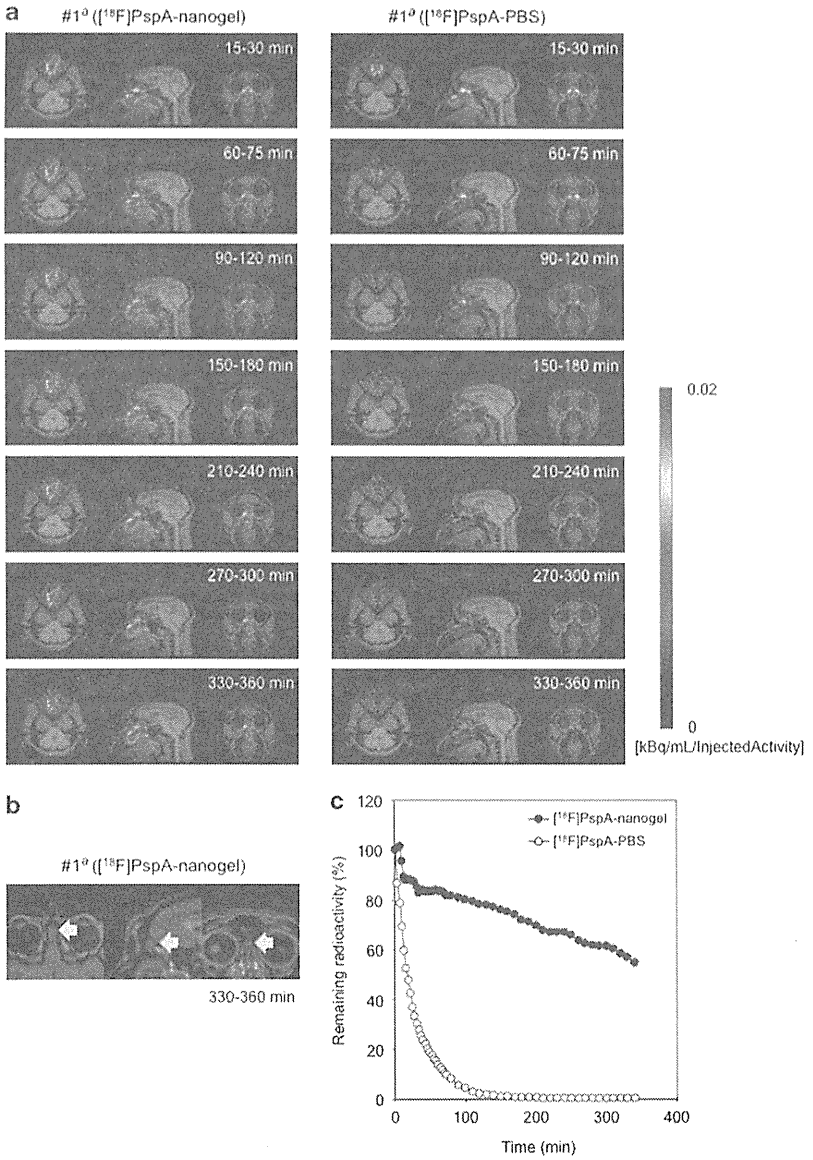

Figure 1 PET/MRI images (**a**,**b**) and TACs (**c**) for nasal administration of [^{18}F]-PspA-nanogel or [^{18}F]-PspA-PBS in a naive rhesus macaque. (**a**) After nasal administration of [^{18}F]-PspA-nanogel or [^{18}F]-PspA-PBS, the macaque's head was scanned for 6 h with a PET scanner. Real-time PET images overlaid on MRI images are shown for the indicated times post-administration. (**b**) To further check whether [^{18}F]-PspA accumulated in the CNS or olfactory bulbs (indicated by arrowheads), PET images taken at 6 h post-administration of [^{18}F]-PspA-nanogel were enlarged. (**c**) TACs for the nasal cavity for 6-h period after nasal administration of [^{18}F]-PspA-nanogel or [^{18}F]-PspA-PBS are presented. The data are expressed as percentages of the dose remaining after nasal administration. *a*: The same macaque was nasally administered of [^{18}F]-PspA-nanogel or [^{18}F]-PspA-PBS with a 1-week interval between administrations. CNS, central nervous system; MRI, magnetic resonance imaging; PET, positron emission tomography; TACs, time-activity curves.

Ab titers revealed that Ab levels gradually decreased over a period of 8 months in macaques nasally immunized with PspA-nanogel. Similarly, PspA-specific bronchoalveolar lavage fluid (BALF) IgG and nasal wash IgA Ab responses exhibited higher levels in macaques nasally immunized with PspA-nanogel when compared with macaques nasally immunized with PspA alone or PBS only (**Figure 2b,c**), and these Ab levels were also gradually decreased. In addition, PspA-specific BALF IgA Ab responses were slightly increased in two of the immunized macaques (#3 and #5) (**Figure 2c**).

When these macaques were given a dose of nasal booster of PspA-nanogel 9 months after the final immunization, the levels of PspA-specific serum and BALF IgG and nasal wash IgA Ab responses immediately recovered to those observed at 9 weeks

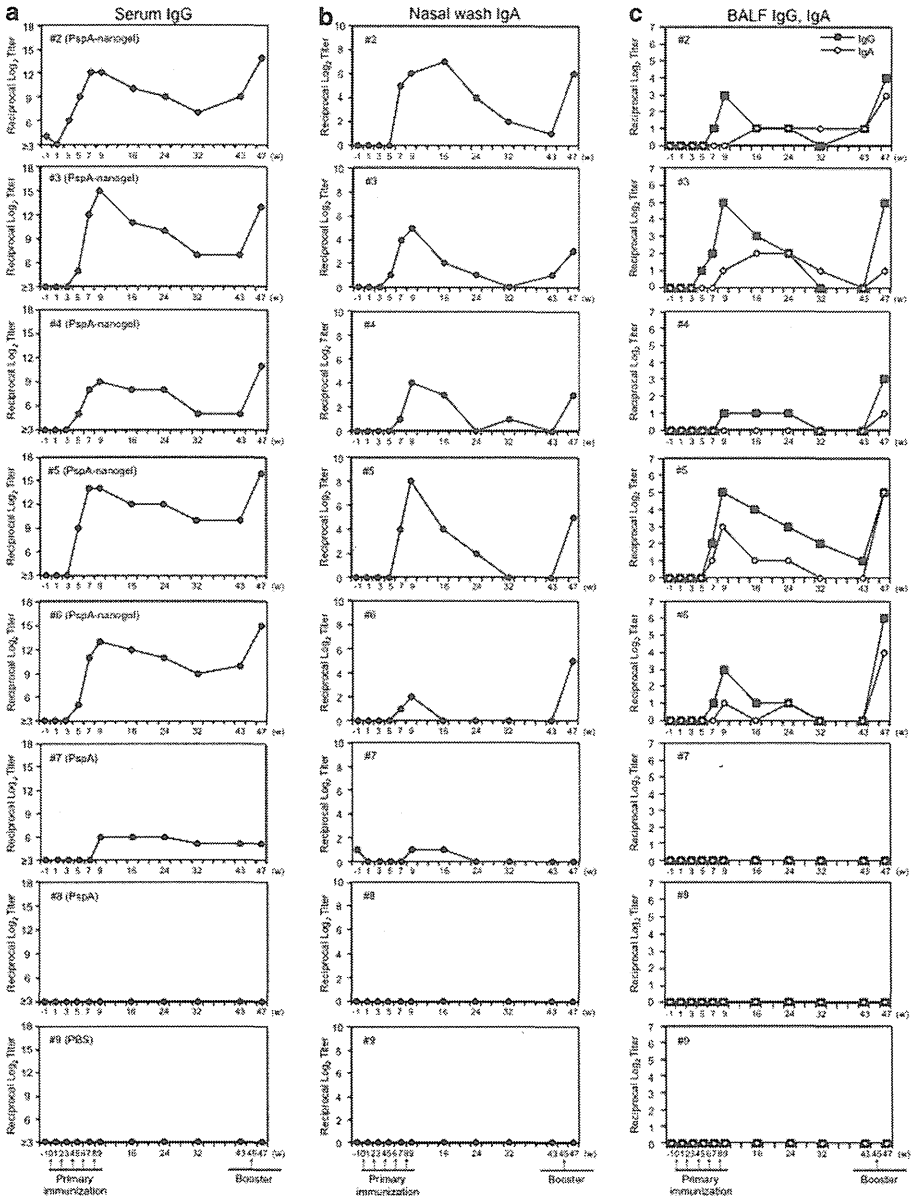

Figure 2 Nasal immunization with PspA-nanogel induced PspA-specific Ab responses in macaques. Each cynomolgus macaque was nasally immunized with PspA-nanogel (macaques #2-#6), PspA alone (#7 and #8), or PBS only (#9) at the times indicated with arrows. Serum, nasal wash, and BALF were collected, and the levels of PspA-specific serum IgG (**a**), nasal wash IgA (**b**), and BALF IgG and IgA (**c**) were determined by ELISA. BALF, bronchoalveolar lavage fluid.

after the initial PspA-nanogel immunization (**Figure 2a–c**). Of importance, a nasal booster induced higher levels of PspA-specific IgA Ab responses in BALF of two macaques (#5 and #6) than those observed after the primary immunization (**Figure 2c**).

These findings suggest that memory-type PspA-specific Ab responses are induced in nonhuman primates after nasal vaccination with PspA-nanogel. PspA-nanogel is therefore a promising nasal vaccine candidate that can induce long-lasting antigen-specific systemic and mucosal immunity and can elicit nasal booster activity in nonhuman primates.

Nasal immunization with PspA-nanogel induces neutralizing Abs against *S. pneumoniae* in macaques

To investigate whether the nasal PspA-nanogel vaccine induced neutralizing Abs, we examined whether PspA-specific serum Abs from macaques nasally immunized with PspA-nanogel would passively protect against pneumococcal infection. CBA/N mice were injected intraperitoneally with diluted pooled sera of macaques nasally immunized with PspA-nanogel, PspA alone, or PBS only. When all groups of mice were challenged with *S. pneumoniae* Xen10 or 3JYP2670 strain via the intravenous route, mice passively immunized with sera